Title

I. LOW TEMPERATURE HEAT CAPACITIES OF VANADIUM, NIOBIUM AND TANTALUM II. LOW TEMPERATURE HEAT CAPACITY OF FERROMAGNETIC CHROMIC TRIBROMIDE

Author

Shen, Yun Lung.

Publication Date

1965-09-01

UCRL-16117

University of California

Ernest O. Lawrence Radiation Laboratory

I. LOW TEMPERATURE HEAT CAPACITIES OF VANADIUM, NIOBIUM AND TANTALUM

II. LOW TEMPERATURE HEAT CAPACITY OF FERROMAGNETIC CHROMIC TRIBROMIDE

Berkeley, California

DISCLAIMER

UCRL-16117

UNIVERSITY OF CALIFORNIA

Lawrence Radiation Laboratory
Berkeley, California

AEC Contract W-7405-eng-48

I. LOW TEMPERATURE HEAT CAPACITIES OF VANADIUM, NIOBIUM and TANTALUM

II. LOW TEMPERATURE HEAT CAPACITY OF FERROMAGNETIC CHROMIC TRIBROMIDE

Yun Lung Shen

September 1965
(Ph.D. Thesis)

CONTENTS

Abstract iii

I. Low Temperature Heat Capacities of Vanadium, Niobium and Tantalum 1

A. Introduction 1

B. Experimental Aspects 4

1. Calorimeter 4

a. Brief Description of Calorimeter 4

b. Thermometry 4

c. Sample Mounting 7

d. Heat Capacity of Copper 8

2. Construction of a Superconducting Magnet 11

3. Residual Resistance Measurements 11

C. Results and Analysis 14

1. Vanadium 14

2. Niobium 20

3. Tantalum 30

D. Discussion 36

1. Mean-Free-Path Effect on Transition Temperature 36

2. Nuclear Heat Capacity 40

3. Lattice Heat Capacity 41

4. Electronic Heat Capacity 47

a. Heat Capacity Discontinuities at the Transition Temperature 47

b. Qualitative Freatures of the Electronic Heat Capacities at Low Temperatures 47

c. Relationship between C_{es} and T_c 49

d. Two Energy Gap Theory at the "Clean Sample" Limit... 50

E. Conclusion and Further Suggestions 57
Tables 58
References 68
Figure Captions 70
II. The Heat Capacity of Ferromagnetic Chromic Tribromide 72
A. Introduction 72
B. Experimental Procedures 73
C. Result and Comparison with Spin Wave Theory 74
Acknowledgements 85
Appendix 86
Tables 87
References 90
Figure Captions 91

I. LOW TEMPERATURE HEAT CAPACITIES OF VANADIUM, NIOBIUM, AND TANTALUM

II. LOW TEMPERATURE HEAT CAPACITY OF FERROMAGNETIC CHROMIC TRIBROMIDE

Yun Lung Shen

Inorganic Materials Research Division, Lawrence Radiation Laboratory
Department of Chemistry, University of California,
Berkeley, California

ABSTRACT

September 1965

I

Experimental studies were made on the heat capacities of vanadium, niobium, and tantalum from 0.3 to 25°K in both normal and superconducting states. Of particular interest is the anomalous superconducting-state heat capacities at low temperatures which are ascribed to the existence of a second energy gap. These measurements constitute the first experimental evidence for the theoretically-predicted second energy in superconducting transition metals. The effect of purity on the superconducting electronic heat capacity was studied, and compared with the electron mean free path via measurements of residual resistances. It is concluded that the lattice heat capacities for these metals are likely to be the same in both normal and superconducting states. Both vanadium and niobium have the same limiting normal-state lattice heat capacities as that determined from the elastic constants.

II

The heat capacity of ferromagnetic chromic tribromide was measured from 0.3 to 25°K in 0, 20.4, and 27 kG magnetic fields. We made use of three parameters: J_t, J_ℓ, and H_A determined from the magnetic properties

of $CrBr_3$ to calculate the magnetic heat capacity from the spin wave theory. The zero-field experimental data agree closely with the calculation from the model of Gossard, Jaccarino, and Remeika between 1 and 2°K where the lattice heat capacity is negligible. Outside this temperature region, the interpretation is less certain. The heat capacity in high magnetic fields deviated considerably from the calculation of the simple theory and an empirical formula was used to fit the data below 4°K.

A. INTRODUCTION

The total heat capacity of a normal metal at low temperature is customarily written as the sum of a lattice, electronic, and nuclear term

$$C_n = C_{\ell n} + \gamma T + C_{nuc} \qquad (1)$$

$$C_{\ell n} = \alpha T^3 + \beta T^5 + \ldots.$$

$$= (12/5)\pi^4 R\ (T/\Theta)^3$$

where γT is the normal-state electronic heat capacity, and $C_{\ell n}$ is the lattice heat capacity. α is related to the Debye characteristic temperature at 0°K, Θ_0, by

$$\alpha = (12/5)\pi^4 R\ \Theta_0^{-3}$$

The assumption that the lattice vibrations that determine Θ are identical with sound waves, identifies Θ_0 as Θ_e, the value that can be calculated from elastic constants. Discrepancies between Θ_0 and Θ_e have been reported for a few metals (including vanadium and niobium), but in most cases the discrepancies have been resolved by improved calorimetric measurements. At the same time the validity of the relation has been questioned on theoretical grounds.[1]

C_{nuc} comes from interaction between the nuclei and electric field gradients or magnetic fields. In this report an external magnetic field H is the only field acting, and C_{nuc} is represented by

$$C_{nuc} = \frac{1}{3}\left(\frac{I+1}{I}\right)\frac{\mu^2\langle H^2\rangle}{k^2T^2} R \quad \text{for } kT \gg \mu H \qquad (2)$$

where I is the nuclear spin, μ is the nuclear magnetic moment, $\langle H^2\rangle$ is the average of external magnetic field over the entire volume of the sample, k is the Boltzmann constant, and R is the gas constant.

In the superconducting state we express the heat capacity as the

sum of a lattice term C_{ls} and electronic term C_{es}

$$C_s = C_{ls} + C_{es} \tag{3}$$

According to the BCS theory of superconductivity,[2] the lattice heat capacity C_{ls} is the same as that of the normal state, and C_{es} is given by

$$C_{es}/\gamma T_c = ae^{-(bT_c/T)} \tag{4}$$

where T_c is the superconducting transition temperature, the parameters a and b are slowly varying functions of T/T_c for $T < T_c/2$, and can be taken as constants within a restricted temperature interval. At low enough temperature C_{es} is vanishingly small, only C_{ls} is left.

One of the many problems in superconductivity is whether C_{ls} equals C_{ln}. Measurements on the change of elastic constants during the superconducting transition indicated that the change is only several parts in 10^5,[3] therefore C_{ls} should equal C_{ln} within the limit of error of calorimetric measurements. But it was discovered experimentally that C_{ls} is less than C_{ln} in indium[4] and this led to a series of theoretical speculations. The extension to other metals of measurements that would test the equality of C_{ls} and C_{ln} is therefore of interest; and vanadium, niobium, and tantalum, are among the metals for which such measurements are possible.

The determination of C_{ls} is possible only if C_{es} becomes a negligible part of the total heat capacity at temperatures for which C_{ls} can still be measured. This condition is fulfilled for metals with high T_c and/or small Θ_0, e.g. indium, lead, mercury, thallium, tin, vanadium, niobium, and tantalum. The last three metals are especially suitable for calorimetric studies at helium-three temperatures because of their relatively

high T_c. Furthermore, for V and Nb elastic constants are available for a comparison with the lattice heat capacity. Earlier results[5,6] indicated that $C_{\ell s}$ might not equal $C_{\ell n}$ or that Θ_o disagreed with Θ_e for V and Nb. In view of the lack of information on the low temperature heat capacities of superconducting V, Nb, and Ta, we undertook measurements from 0.3 to 25°K in a He^3 cryostat to test whether $C_{\ell s}$ is equal to $C_{\ell n}$.

Secondly, an extension of the BCS theory to transition metals with s- and d-energy bands by Suhl, Walker, and Matthias[7] shows that the temperature dependence of C_{es} might be more complicated than the BCS expression. Investigation of C_{es} on very high purity materials in the region $T << T_c$ might reveal the effect of extreme energy gap anisotropy. Niobium has the highest T_c among pure metals except radioactive technetium, hence, it is suitable for experimental studies of this effect.

Experiments on both heat capacities and residual resistances are described in Section II. Section III contains heat capacity data as well as a conventional analysis for each of the three metals. In this analysis we assume that $C_{\ell s} = C_{\ell n}$ and this point will be justified in Section IV which is denoted to a discussion of the results and a comparison with theory.

B. EXPERIMENTAL ASPECTS

1. Calorimeter

a. Brief Description of Calorimeter

A calorimeter that used He^3 to reach temperatures below 1°K and which can also be used above 4°K was used in all heat capacity measurements. Temperature measurements were made with a low-resistance (35 ohms at 4.2°K) thermometer. Details of the construction of the apparatus were described by N. M. Senozan,[8] and will be only briefly mentioned here.

Cooling to 0.25°K was accomplished by pumping on liquid helium-three with a 4-inch diffusion pump. The sample was isolated thermally by mechanical motion of the heat switch in a vacuum space that was immersed in liquid helium-4. A measured amount of energy was put in via a resistance heater that was attached to the sample, and the temperature rise of the sample was recorded potentiometrically from the resistance change of the germanium thermometer.

Superconducting-state heat capacities were measured after the sample was cooled down in 1/30 earth field. This was the residual field inside a mu-metal shield placed outside the dewar. The sample was surrounded with a superconducting magnet that could drive the sample into the normal state. Heat capacities up to 25°K could be measured both with and without an external magnetic field.

b. Thermometry

A germanium resistance thermometer was mounted on the sample holder and calibrated from 0.3 to 25°K as previously reported.[8] The germanium thermometer was reproducible on thermal cycling to better than the accuracy of temperature determination. The thermometer on which all

measurements were based, was recalibrated against the vapor pressure of liquid helium ten months after its original calibration without any observable difference. In the same period, the germanium thermometer on the sample was compared repeatedly with another calibrated germanium thermometer on the He^3 block from 0.3 to 25°K and agreed with the original calibration.

The thermometer resistance was determined by measuring the D. C. voltage across the two potential leads with a measured current flowing. The thermal E.M.F. remained nearly constant and small (0.1 micro-volt) in each run. Since dR/dT is small for a low resistance thermometer, a higher thermometer current had to be used at higher temperatures (0.1 ma. at 25°K). The heating effect of thermometer current was measured by Senozan,[8] and care was always taken to let the thermometer operate in a region where its resistance was power-independent.

The resistance vs temperature calibration table was based on the following:

0.3 to 1.1°K - Magnetic susceptibility of cerium magnesium nitrate crystal, extrapolated from above 1°K.

1.1 to 4.2°K - Helium-4 vapor pressure scale (1958). A vapor pressure bulb was used for calibration from 2.2 to 4.2°K, and below 2.2°K the pressure above the bath was measured. With helium exchange gas inside vacuum can, no calibration discontinuity appeared near the lambda point of helium.

10 to 25°K - Platinum resistance thermometer (calibrated by NBS).

4.2 to 10°K - Interpolation of the resistance of an Allen-Bradley radio resistor which was calibrated below

4°K against He^4 vapor pressure and above 10°K against the Pt thermometer.

To make use of a computer to calculate heat capacities and to smooth out random errors in thermometer calibration, we fit the calibration data to

$$1/T = k_o + k_1 \log R + k_2(\log R)^2 + k_3(\log R)^3 + k_4(\log R)^4 + k_5(\log R)^5. \quad (5)$$

From 2.5 to 25°K the fit was better than 1% in T. For each calibration point we had a calculated temperature and an observed temperature. Their fractional difference was plotted as a function of calculated temperature, and a smoothed curve, called the "difference plot", was drawn through the points. The "difference plot" was fed into the computer so that for each resistance value the machine calculated a temperature corresponding to the observed temperature. Equation (5) fit calibration data between 0.3 and 3°K to within 0.1%, and we used a straight line for the difference plot. An attempt to fit R vs T over the whole temperature range with up to 15 parameters failed to give satisfactory results. The present method did not introduce error as long as the two "difference plot" were made to join smoothly.

The thermometer calibration with maximum current flowing in the superconducting magnet was also checked by comparison with another germanium thermometer outside the magnetic field. We observed no detectable change on calibration from 0.46 to 25°K with about one kilogauss field on the thermometer. Below 0.46°K which represented the lowest operating temperature for our electronic temperature regulator, the calibration encountered the difficulty of having a thermal gradient between the two germanium

thermometers due to eddy current heating from the superconducting magnet. Even though the created temperature difference was only two millidegrees, the calibration became less accurate. An upper limit to the thermometer resistance change was set at 0.5% at the lowest temperature with 27.7 kG at the center of the solenoid.

c. Sample mounting

The sample was supported by cotton threads attached to two copper rings which were clamped on the sample by copper screws. One of the rings carried the thermometer and a copper wire that led to the heat switches. A manganin resistance heater was wound on a third copper ring. Thermal contact between the sample and the rings was improved by applying about two milligrams of Apiezon vacuum grease between the sample and the copper rings. Apart from Tantalum I and Niobium III, all samples were $\frac{1}{2}$"-diameter, 4"-long, rod which could be slid in and out of the sample holder without demounting the rings. The addenda consisted of approximately 5 g of copper, 0.03 g manganin, a Minneapolis Honeywell, type MHSP-4401 germanium thermometer of special low resistance, and unmeasured but small (less than 100 mg) amounts of G.E. 7031 varnish and silver solder. The heat capacity of addenda was measured by attaching the rings to a thin-walled, high-purity, copper tube. Another check on the heat capacity of addenda was made by W. R. Gardner of this laboratory ten months after the first addenda run with the same result. We represent the addenda correction by the following equation

$$C_{\text{addenda}} = 0.0622\ T + 0.00879\ T^3 - 0.33 \times 10^{-5}\ T^5 + \frac{0.802 \times 10^{-3}}{T^2}\ \text{mJ/°K.}$$

In the superconducting state, the heat capacities of all three metals at 0.3°K were so small that the movement of the mechanical heat switch

created enough heat to raise the sample temperature by several hundred millidegrees. However, vibration heat-leak into the sample was small, in most cases, that the sample cools down in approximately two hours to 0.3°K by losing its thermal energy to the surroundings even when the heat switch was completely open. No such heating difficulties were encountered in the normal state measurements because of the large γT term in the heat capacity.

The manganin heater resistance was measured as a function of temperature and was represented by the equation

$$1042.0 + 0.34\ T + 0.015\ T^3 - 3.7 \times 10^{-5}\ T^3 \text{ ohms.}$$

We have found that the heater resistance decreased in high magnetic field by approximately 0.5% and showed less temperature dependence. This effect is presumably due to the alignment of the magnetic ions with the high magnetic field, rendering the ions to be less effective scattering centers for the conduction electrons.

d. Heat capacity of copper

Copper has been measured by a number of investigators over various temperature ranges. We measured a 2.22-mole sample (99.9999 pure) in order to check the thermometer calibration from 0.3 to 25°K. The same sample was measured by J. C. M. Ho down to 0.1°K.[9] A plot of C/T vs T^2 is shown in Fig. 1. The best fit to the data is given by

$$C = 0.696\ T + 0.04785\ T^3 \text{ mJ/mole-°K}$$

from 0.3 to 4.2°K. The points above 4.2°K are plotted as Θ vs T together with results by Martin et al.[10] in Fig. 2.

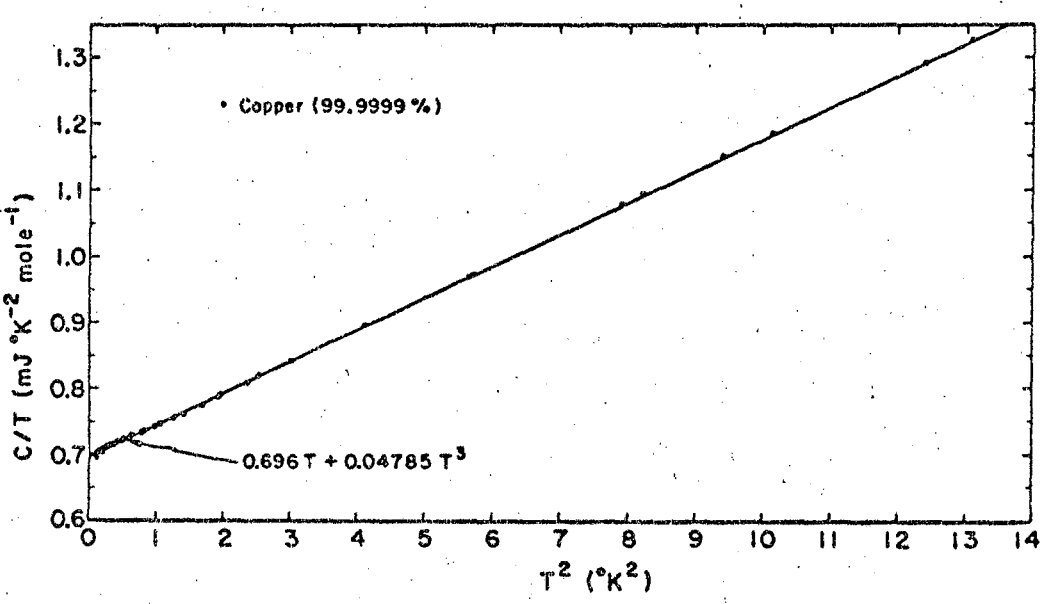

Fig. 1

Heat capacity of copper between 0.3 and 4 °K.

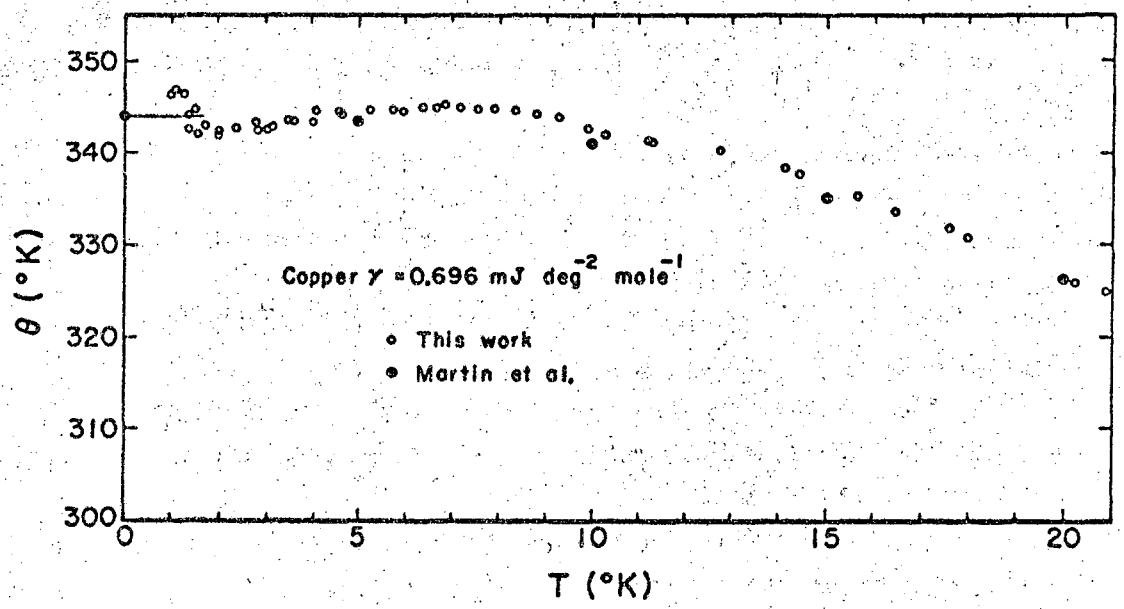

Fig. 2

Variation of the Debye temperature of copper with temperature.

2. Construction of a Superconducting Magnet

In order to apply a homogeneous high-magnetic field to the sample during heat capacity measurements, a solenoid was wound with copper-clad, Nb-Zr wire supplied by Westinghouse Corporation. The magnet is 3"-O.D., 1.3"-I.D. and 6" in length. Its crossection is shown in Fig. 3. It consists of two concentric solenoids connected in series. The Formvar-coated wire is wound on copper-plated stainless steel tube. Mylar tape acts as layer to layer insulation. The outer solenoid contains compensating coils designed to obtain a uniform field region up to 2.5" long with spatial variation of field less than 1%.

The ends of the Nb-Zr wire were tinned ultrasonically first and soldered to heavy copper wires that fed current to the superconducting solenoid. The magnetic field inside the magnet was measured by a flux integrating device that agreed with the calculated field which is 1510 gauss/ampere.

3. Residual Resistance Measurements

A simple D.C. potentiometric method was used to measure the residual resistance ratio $R_{300}/R_{4.2}$ for the vanadium, niobium, and tantalum samples. In order to obtain a D.C. potential that is more than one microvolt at 4.2°K in the normal state, we passed a measuring current of 10 amperes through the whole length of the sample by means of a spring-loaded mechanical copper contact. Potential leads were taken directly from the surface of the sample, (See Fig. 3). The superconducting state was quenched at 4.2°K by the same magnet as described in the preceding section. Resistances were measured in different magnetic fields and extrapolated to zero field value to eliminate magnetoresistance. This correction was

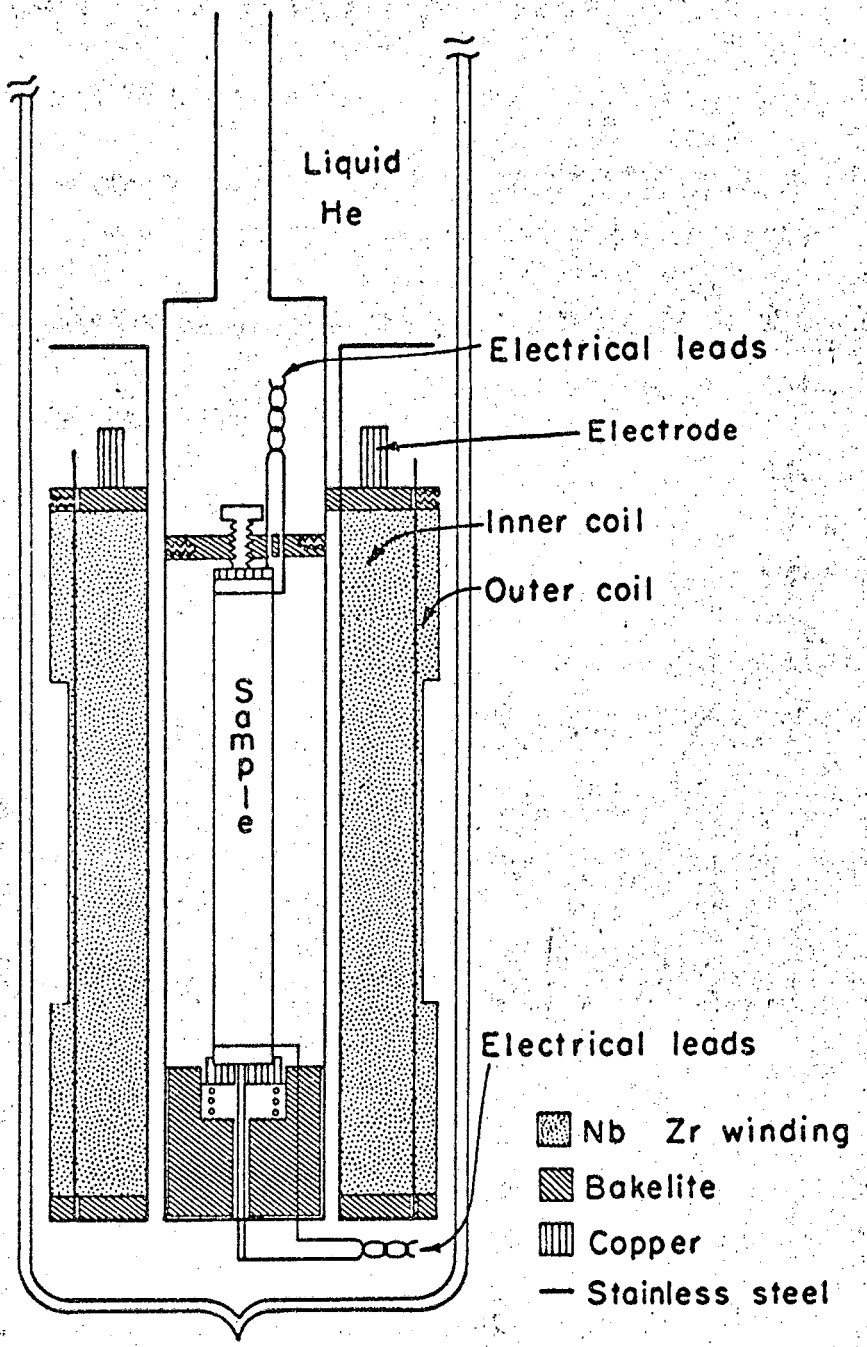

Fig. 3

The system for measuring residual resistivity. The same superconducting magnet was used in the heat capacity measurements.

never greater than 5% even in our purest niobium sample. The room temperature resistance was taken as the averaged value before and after cooling. All thermal E.M.F. corrections were not significant as compared with the readings.

C. RESULTS AND ANALYSIS

Table I summarizes the properties of the samples and the results of the residual resistance measurements. The experimental data are analyzed according to Eqs. (1-4), with the further assumption that $C_{\ell s} = C_{\ell n}$. This assumption will be discussed in Sec. IV.

1. Vanadium

The measurements were made on two cylindrical single crystals. Table II gives the abundances of the various impurities. Apart from a small difference in T_c, both samples yield identical results. The normal-state heat capacity below 4.2°K could be represented by

$$C_n = 0.041/T^2 + 9.64\ T + 0.030\ T^3 \quad \text{mJ/mole-°K}$$

The T^{-2} term was determined by plotting CT^2 vs T^3 for the below -1°K data. The intercept in this plot gives the T^{-2} coefficient. The calculated C_{nuc}, from the interaction of the nuclear moment (5.1 nm., 99.8%; 3.3 nm., 0.2%) with the 22 kG applied field is $.0042\ T^{-2}$. This is a satisfactory agreement since C_{nuc} is only 10% of C_n at the lowest temperatures and $\langle H^2 \rangle$ is not accurately known.

Approximate values of the T and T^3 coefficients were found by plotting C_n/T vs T^2 as shown in Fig. 4. The straight line that passes the normal state data represents C_n less the nuclear contribution, and its intercept and slope correspond to $\gamma = 9.64$ mJ/mole-°K^2, $\alpha = 0.030$ mJ/mole -°K^4, respectively. Finally we obtain γ, α, and β by plotting $(C_n - \gamma T)/T^3$ vs T^2 for different γ's in Fig. 5. The intercept in this graph is α and the slope if β. Figure 5 also shows the value of α_e corresponding to the elastic constants. It is found from Fig. 5 that (1) a small change of γ

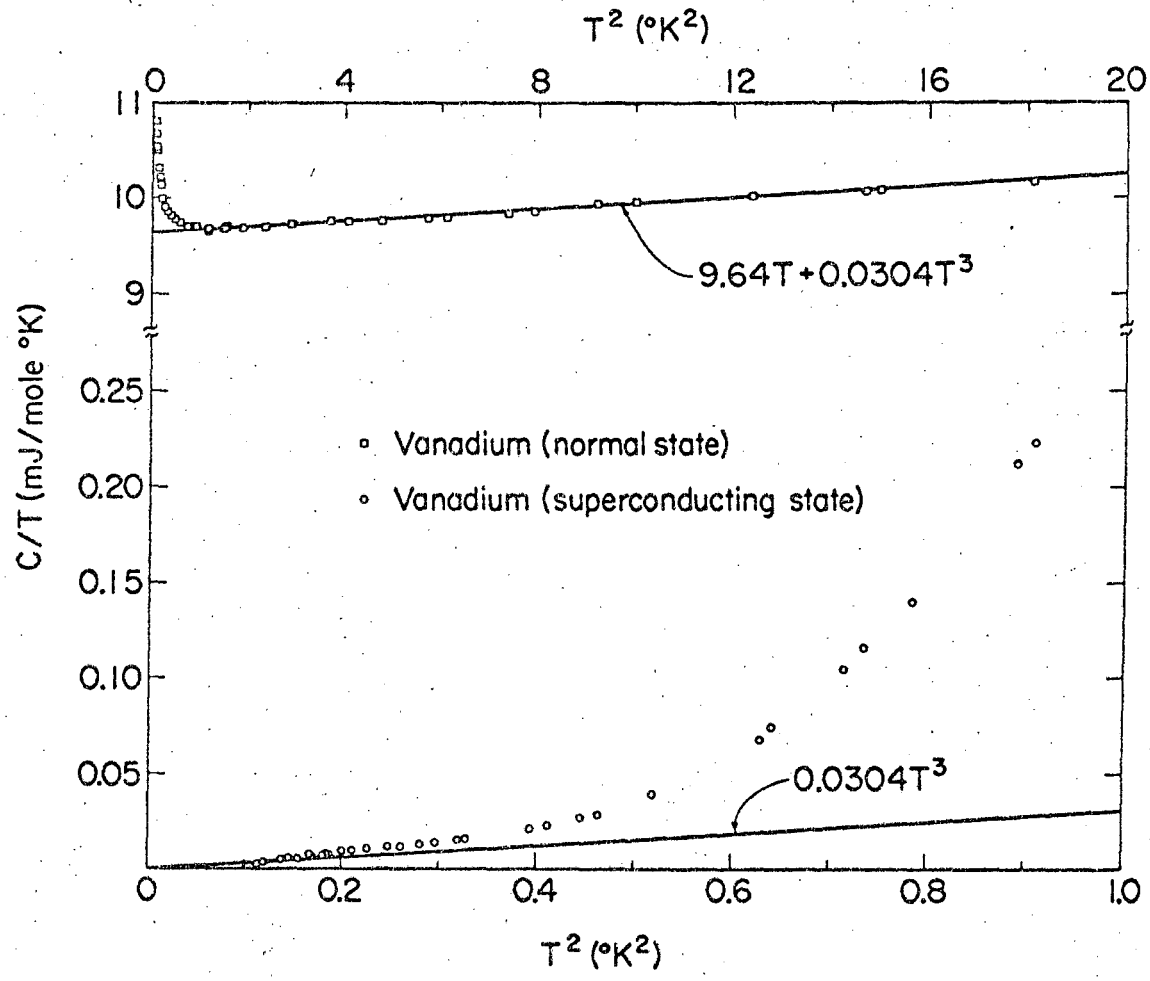

Fig. 4

The heat capacity of vanadium. The slopes of the solid lines represent $C_{\ell n}$.

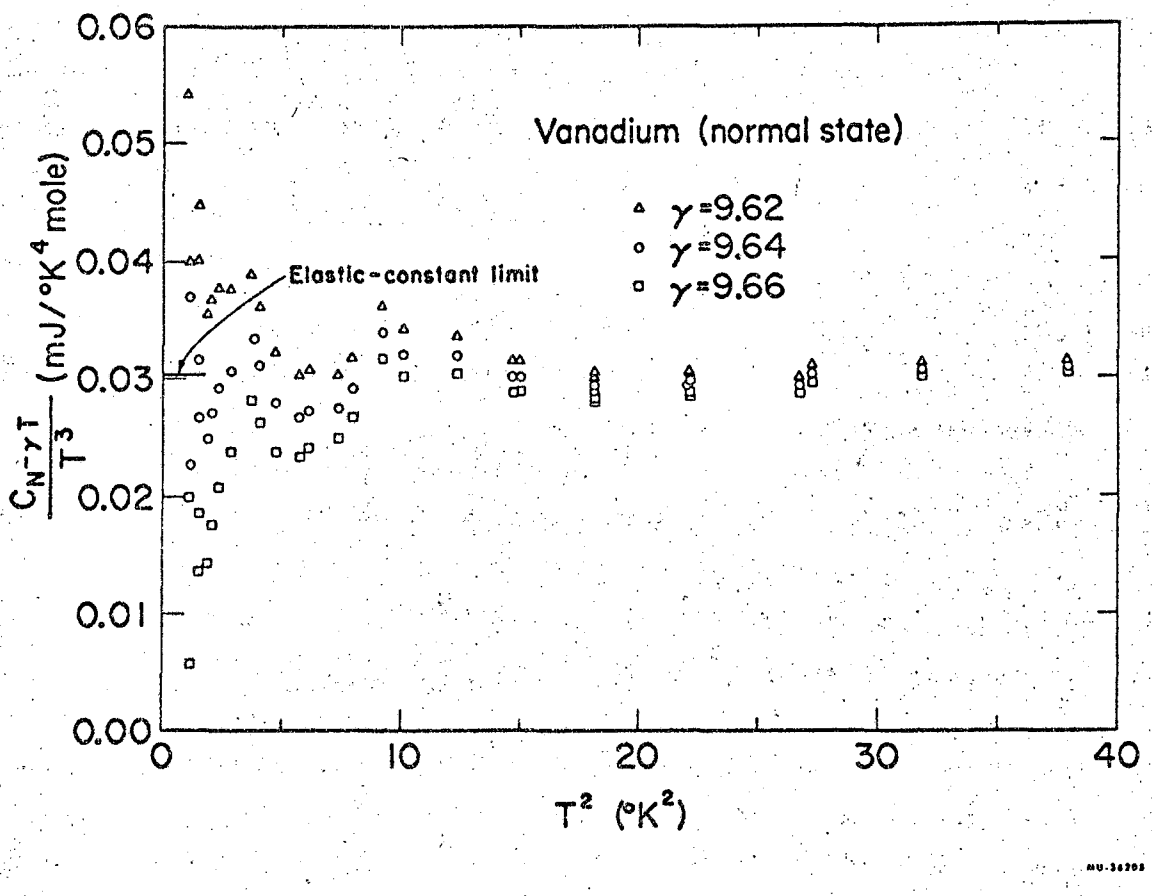

Fig. 5

The heat capacities of two different vanadium samples near the transition temperature.

from the value 9.64 mJ/mole-°K^2 distorts the expected linear behavior of the experimental data; (2) calorimetric α agrees with that determined from elastic constants within the relatively large experimental error, since $C_{\ell n}$ is a small fraction of C_n in the low temperature region; (3) $C_{\ell n}$ contains no observable T^5 term below 4.2°K.

Figure 6 shows heat capacities taken with small temperature increments (about 5 millidegrees) for the purpose of determining the temperature and width of the superconducting transition. The transition is complete within an interval of 0.1°K and is centered at 5.084°K for Vanadium I and 5.068°K for Vanadium II. The difference in heat capacities between the normal and superconducting states at T_c is $(C_s-C_n)/\gamma T_c = 1.50$. See Table III.

Below 1°K, C_s is plotted in Fig. 4 together with a straight line that represents C_n. It is clear that at low temperatures C_s approaches $C_{\ell n}$. Figure 7 shows a semi-logrithmic plot of the experimental $C_{es}/\gamma T_c$ vs T_c/T, where $C_{es} = C_s - 0.0304\ T^3$. From Eq. (2), a and b are determined as 7.86 and 1.43, respectively, for $2 < T_c/T < 6$. The value of b corresponds to an energy gap $2\Delta(0) = 3.5\ kT_c$ at 0°K. Possible explanations of the positive deviation from the BCS theory for T/T_c less than 0.2 is presented in Sec. IV.

Smoothed experimental values of C_s, extrapolated to T = 0°K, were used to calculate free energy difference between the normal and superconducting states, $\Delta F(T)$, and the critical field $H_c(T)$, according to the thermodynamic relation

$$\Delta F(T) = \frac{V_m H_c(T)}{8\pi} \int_{T_c}^{T} dT \int_{0}^{T} \left(\frac{C_n - C_s}{T} \right) dT \qquad (6)$$

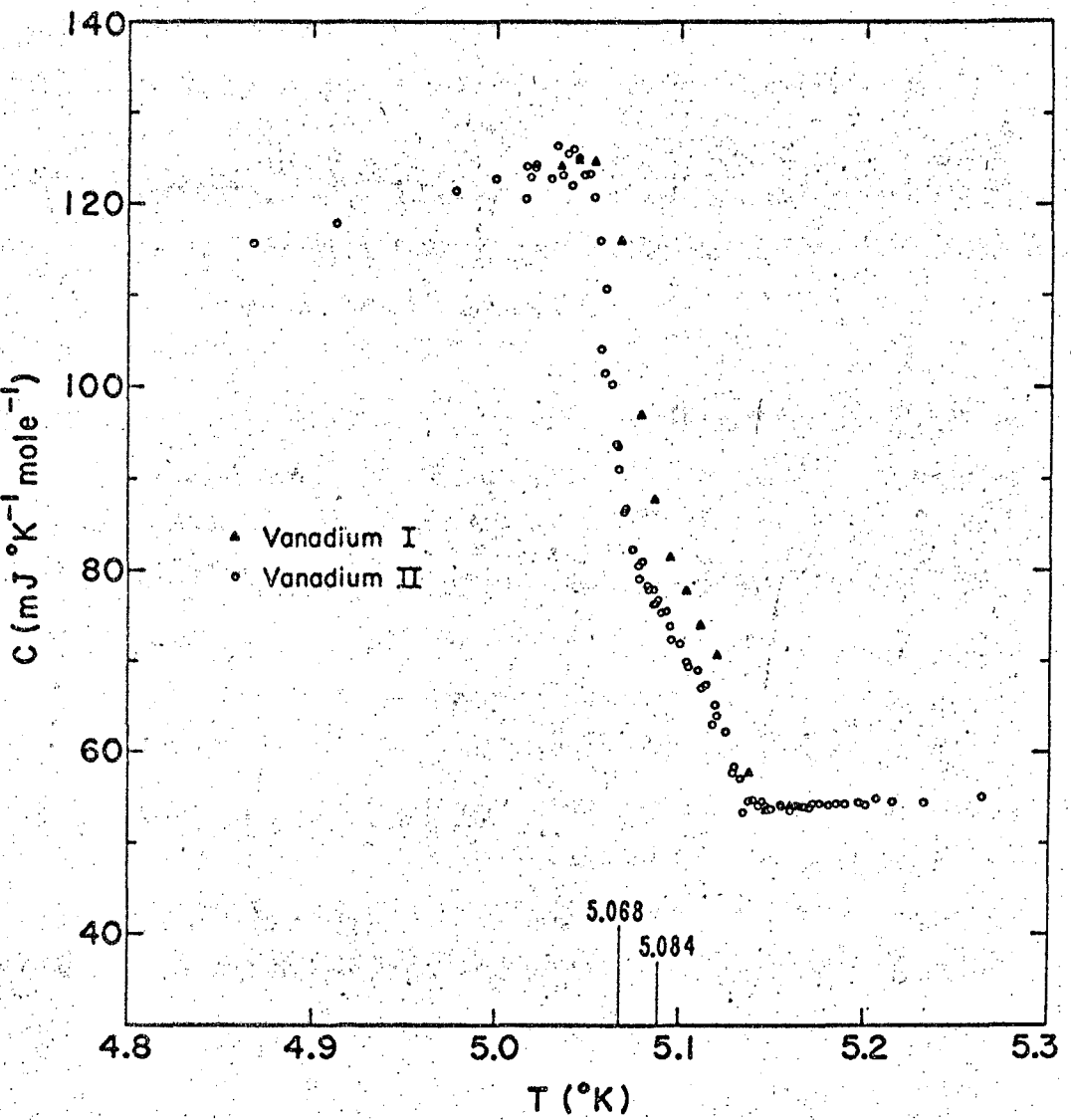

Fig. 6

The superconducting-state electronic heat capacity of vanadium.

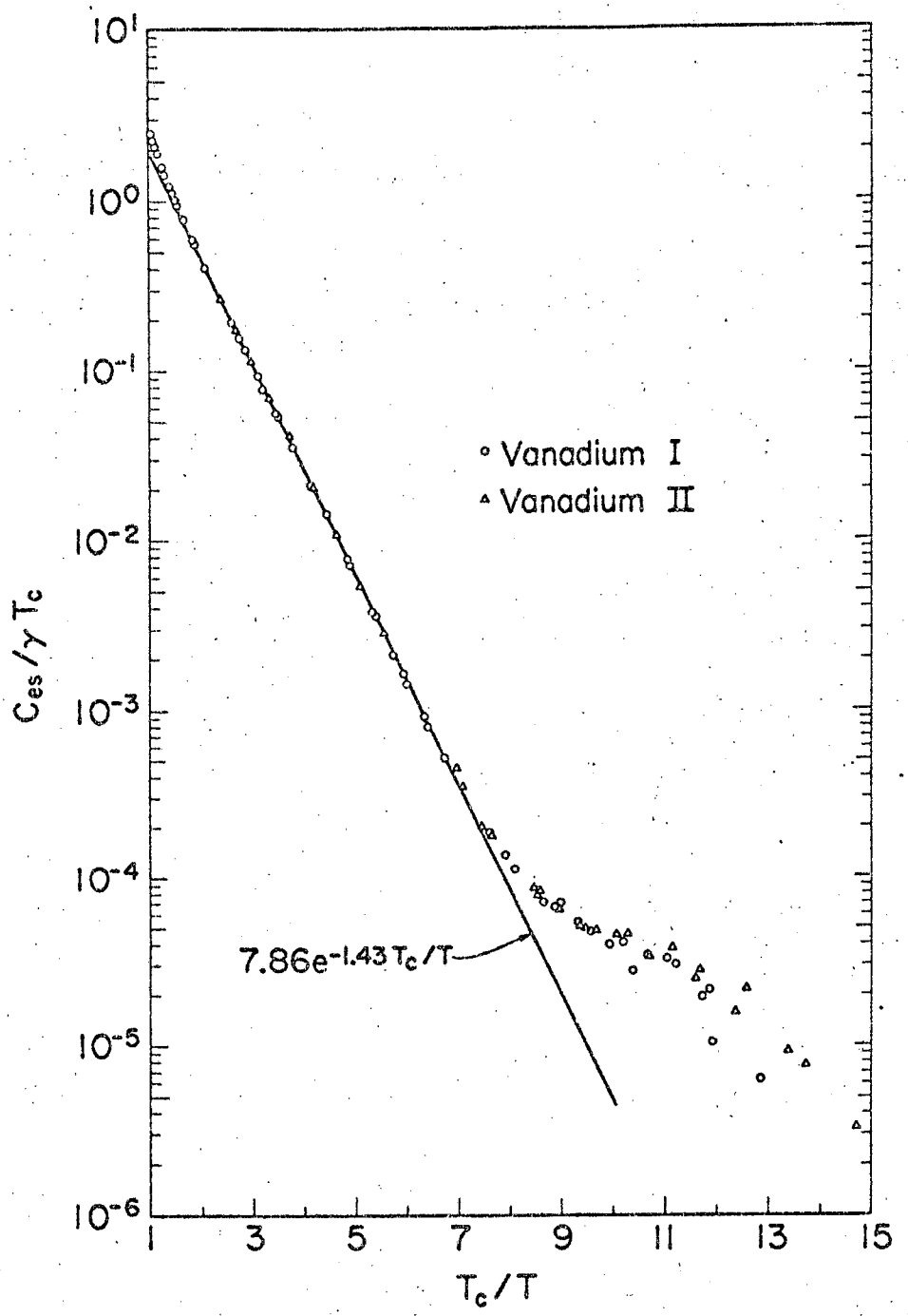

Fig. 7

The lattice heat capacity of normal vanadium.

where V_m is the molar volume at 0°K(8.435 cm^3/mole).[11] For this purpose T_c is chosen to be 5.118°K, at which the entropy difference vanishes. The deviation of the critical field from parabolic temperature dependence, $D(t) = h - (1-t^2)$, is shown in Fig. 8 as a plot of $D(t)$ vs t^2, where the reduced temperature $t = T/T_c$, and $h = H_c(T)/H_c(0)$.

The value of the energy gap can also be estimated from the BCS relation

$$\frac{2\Delta(0)}{kT_c} = \frac{4\pi}{\sqrt{3}} \left(\frac{H_c(0)^2 V}{8\pi\gamma T_c^2} \right) \qquad (7)$$

and the experimental values of $H_c(0)$ and T_c.[12] For vanadium, the value of $2\Delta(0)$ was calculated as 3.56 kT_c from the above equation.

Table IV summarizes the comparison of our data with other related measurements on vanadium. Different grade samples as well as differences in temperature measurements above 4.2°K probably account for the different values of T_c. γ is a very impurity-sensitive quantity for many metals. The highest residual-resistance-ratio sample for which measurements have been reported, is that of Keesom and Radebaugh[13] who reported $\gamma = 9.92$ mJ/mole-$°K^2$.

2. Niobium

We have extended previous work by N. M. Senozan[8] of this laboratory (his sample is later referred as Nb I) to include measurements on niobium of different purities. Nb II was a 99.9%-pure, polycrystalline sample of material similar to that from which the single-crystal Nb I was prepared by triple zone-refining. Nb II was vacuum-annealed at 1000°C and 10^{-5} mm Hg pressure for 24 hours before the measurements. Nb III was a 1/4" O.D., 6" long, cylindrical, zone-refined single crystal. In this

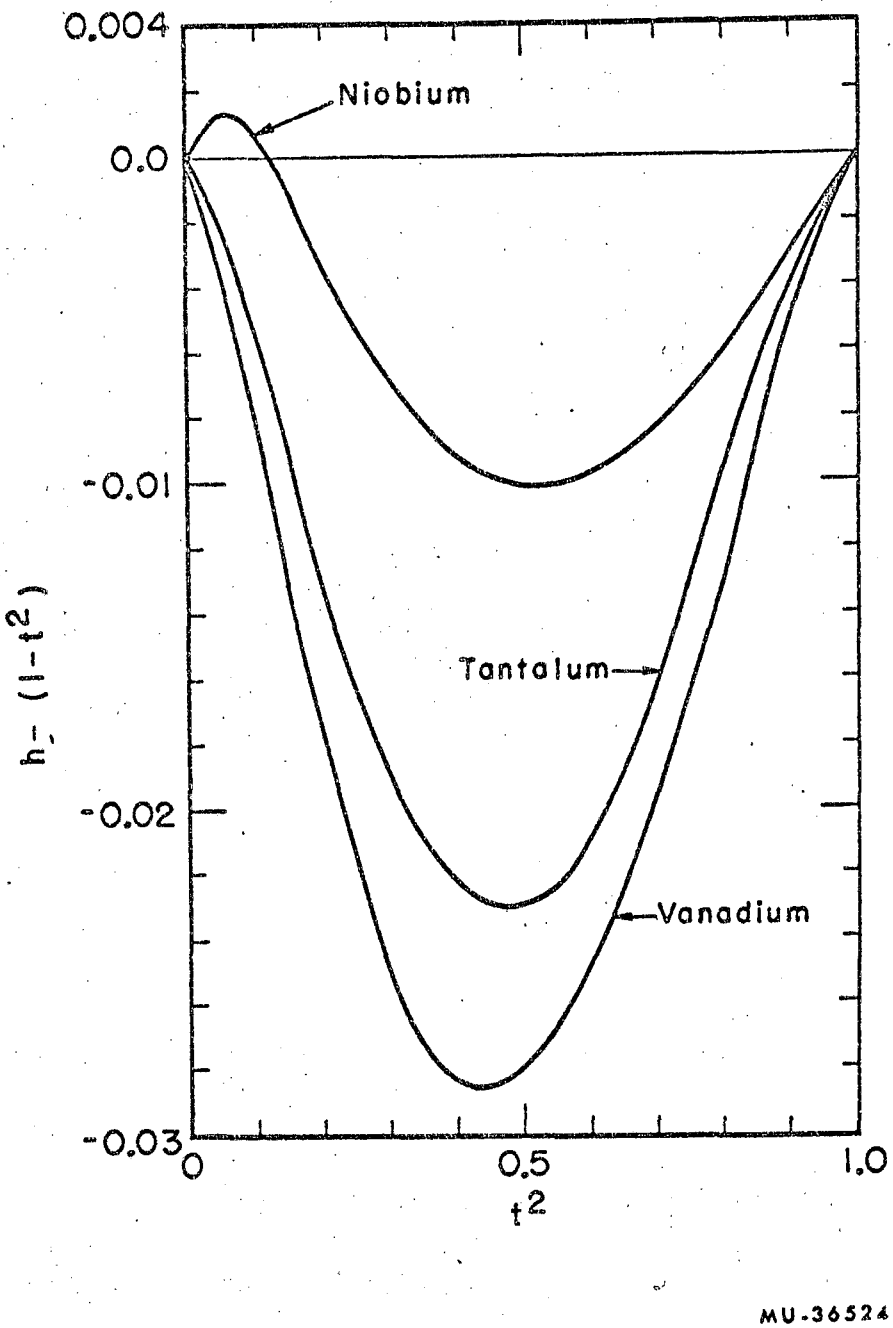

Fig. 8

The deviations of the critical fields of vanadium, niobium, and tantalum from a parabola.

case we used three additional copper rings, that constituted an addition to the addenda, to accommodate Nb III in the sample holder. Nb IV differed from Nb I only by the orientation of its crystalline axis. Nb IV was later annealed at 1200°C and 10^{-4} mm Hg pressure for 24 hours, and was called Nb V after annealing. Nb VI was a pure, polycrystalline, zone-refined rod. The alloys Nb-Fe (100 ppm Fe) and Nb-Zr (1000 ppm Zr) were prepared by doping samples similar to Nb VI. A neutron activation analysis was carried out on Nb I, Nb II, and Nb III. The results of this analysis are presented in Table V together with analyses reported by the suppliers of the samples.

For all eight niobium samples that we studied the mean-free-paths were longer than the coherence distance (See Sec. D), which implies that the samples were quite "clean". However, in order to simplify our description three classes of samples are distinguished on the basis of their low-temperature C_{es}. Nb I and Nb IV belonged to the "clean class" which had the highest low-temperature C_{es}. Nb II, Nb V, Nb VI, Nb-Fe, and Nb-Zr belonged to the "dirty class" which had the lowest low-temperature C_{es}. Nb III stood out as the intermediate case. The nomenclature of "clean" and "dirty" was used to indicate the relative purity of the samples and will be discussed again in Sec. D. The results of the representative cases Nb I, Nb II, and Nb III, will be presented in detail here. (This classification into "clean" and "dirty" samples is consistent with the one based on residual resistances and known impurities for the tantalum samples, but for niobium there are some inconsistencies which will be discussed later.)

C_n is essentially the same for all samples. We can represent the normal-state heat capacity of Nb II in 24 kG field by

$$C_n = 0.085/T^2 + 7.79\ T + 0.0915\ T^3 + 0.001\ T^5\ \text{mJ/mole-°K.}$$

The T^{-2} term was determined by plotting CT^2 vs T^3 for the below 1°K data. $\alpha = 0.0915$ mJ/mole-°K^4, $\beta = 0.001$ mJ/mole-°K^6 are taken from the report on Nb I by N. M. Senozan.[8] γ changes slightly (less than 1%) from sample to sample. For Nb II $\gamma = 7.79$ mJ/mole-°K^2, and for both Nb I and Nb III $\gamma = 7.85$ mJ/mole-°K^2.

The parameter γ which characterizes C_n for all eight niobium samples are listed in Table VI. Within the experimental error, Θ_o is the same for all samples and agrees with Θ_e. Figure 9 shows C_n/T plotted vs T^2 with a straight line that best represents C_n data for Nb I below 3°K. The C_n of Nb I, Nb II, and Nb III are all presented in Fig. 9. In the cases of Nb I and Nb III, the applied fields were not great enough to make the whole sample normal below 1°K. Hence, only the results of Nb II are given in that temperature region.

Figure 10 shows the heat capacities taken with small temperature increments (about 5 millidegrees) near T_c. T_c is equal to 9.287°K for Nb III, 9.261°K for Nb I, and 9.128°K for Nb II. Table VI presents a complete list of T_c, the maximum width of transition, and $(C_s-C_n)/\gamma\ T_c$ of other niobium samples. $(C_s-C_n)/\gamma\ T_c$ has been determined to be 1.80 at T_c for Nb I.

Below 1°K, C_s is plotted in Fig. 9 together with a straight line that represents $C_{\ell n}$ for all samples. C_s of the "dirty class" samples is close to that of Nb II. For some of these "dirty" samples, C_s is closer to $C_{\ell n}$ but for all of them it remains slightly above. C_s for the other sample of the "clean class" was essentially the same as that of Nb I. The difference between the "clean" and "dirty" classes is clearly demonstrated

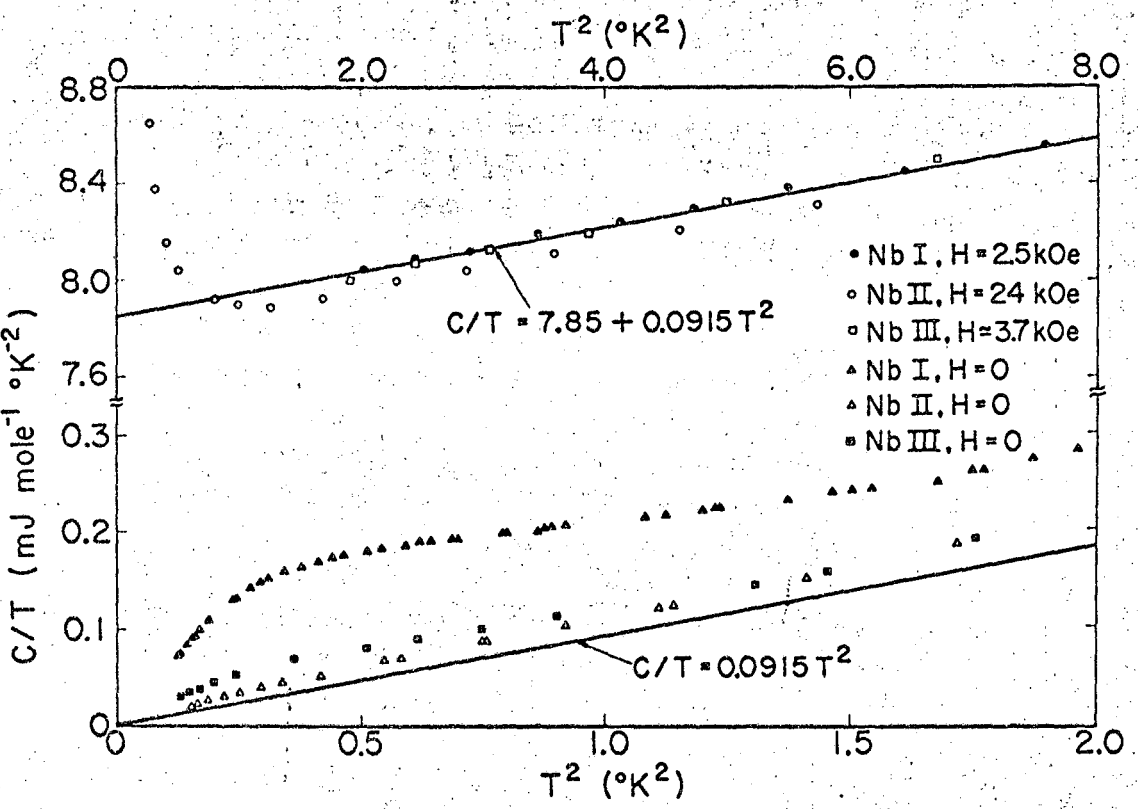

Mub - 5943

Fig. 9

The heat capacities of different-purity niobium samples. The slopes of the solid lines represent $C_{\ell n}$.

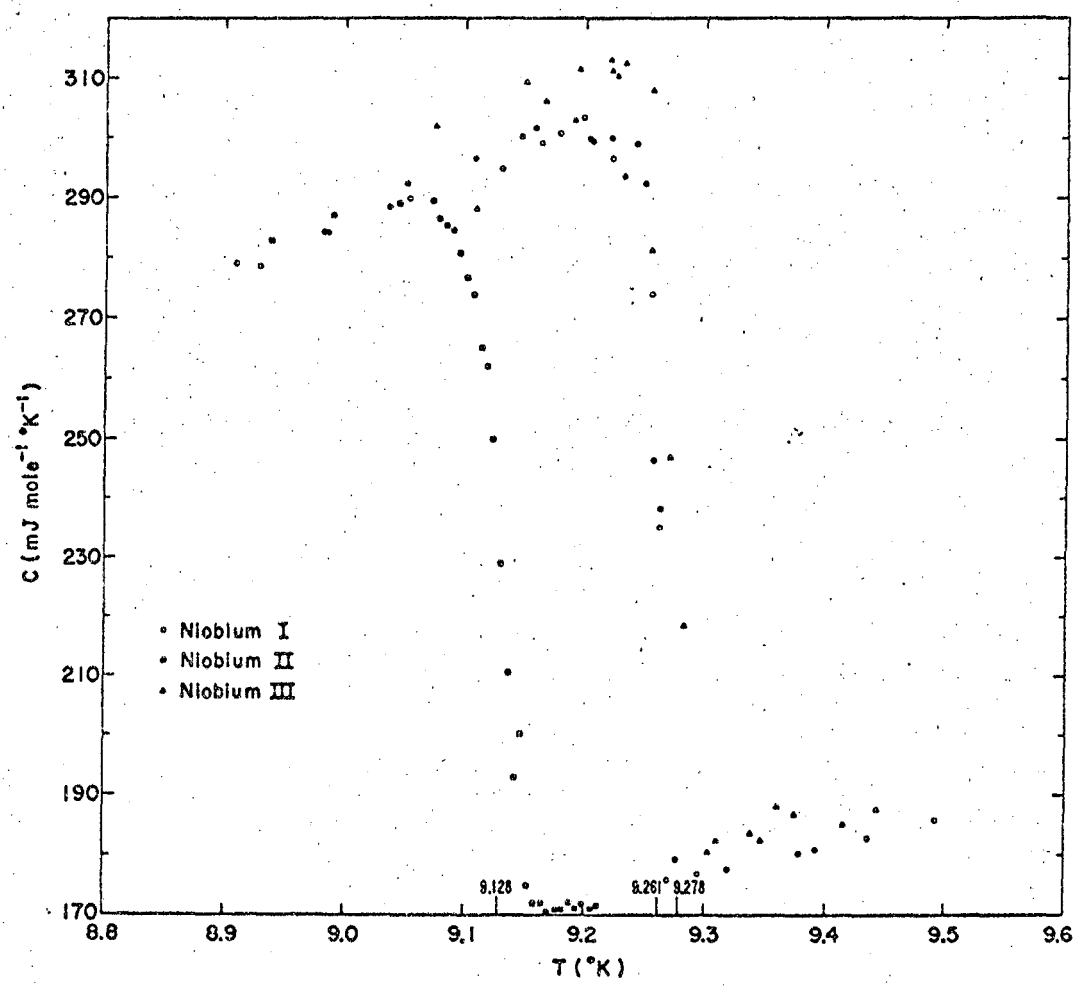

Fig. 10

The heat capacities of three niobium samples near the transition temperature.

when Nb IV of the clean class transferred to Nb V of the dirty class by picking up 5 mg of gaseous impurities during annealing at 1200°C and 10^{-4} mm Hg pressure of air. The residual resistivity ratio $R_{300}/R_{4.2}$ of Nb IV decreased from 110 to 61 during this process.

C_{es}'s for Nb I, Nb II, and Nb III are shown in Fig. 11 where we plot $C_{es}/\gamma T_c$ vs T_c/T by taking $C_{es} = C_s - 0.00915\ T^3 - 0.001\ T^5$. Between T_c and $T_c/6$, $C_{es}/\gamma T_c$ is essentially the same for Nb I, Nb II, and Nb III; and is given by $C_{es}/\gamma T_c = 7.0 \exp(-1.46\ T_c/T)$ for $2 < T_c/T < 6$. For $T < T_c/14$, $C_{es}/\gamma T_c$ is proportional to $\exp(-0.12\ T_c/T)$ but the proportional constants are 0.0066, 0.0018, and 0.00065 for Nb I, Nb III, and Nb II, respectively. At intermediate temperatures $C_{es}/\gamma T_c$ is less than the sum of the corresponding exponential terms for all samples, but the discrepancy is especially pronounced for both Nb I and Nb III. Nb II appears to be near the "dirty sample limit" because the other four samples of the "dirty class" are similar to Nb II even though the nature and the quantity of impurities are quite different. Figure 12 shows $C_{es}/\gamma T_c$ vs T_c/T for Nb IV, Nb V, Nb VI, Nb-Zr and Nb-Fe.

From Eq. (6) we calculated the critical field of Nb I, using $V_m = 10.79$ cm^3/mole at 0°K.[11] T_c was chosen to be 9.257°K at which the entropy difference vanished. $H_c(0)$ was found to be 1995 G, in excellent agreement with the field deduced from calorimetric measurements by Leupold and Boorse[14] who found the value to be 1994G, and by McConville and Serin,[15] 1990G. The value obtained from direct magnetic measurements by Stromberg and Swenson[16] was 1960±40G. Figure 8 shows the plot of D(t) vs t^2 for Nb I. The unusual temperature dependence of D(t), which has both positive and negative values, was also found by Leupold and Boorse,[14] who explained this behavior in terms of Swihart's calculation of

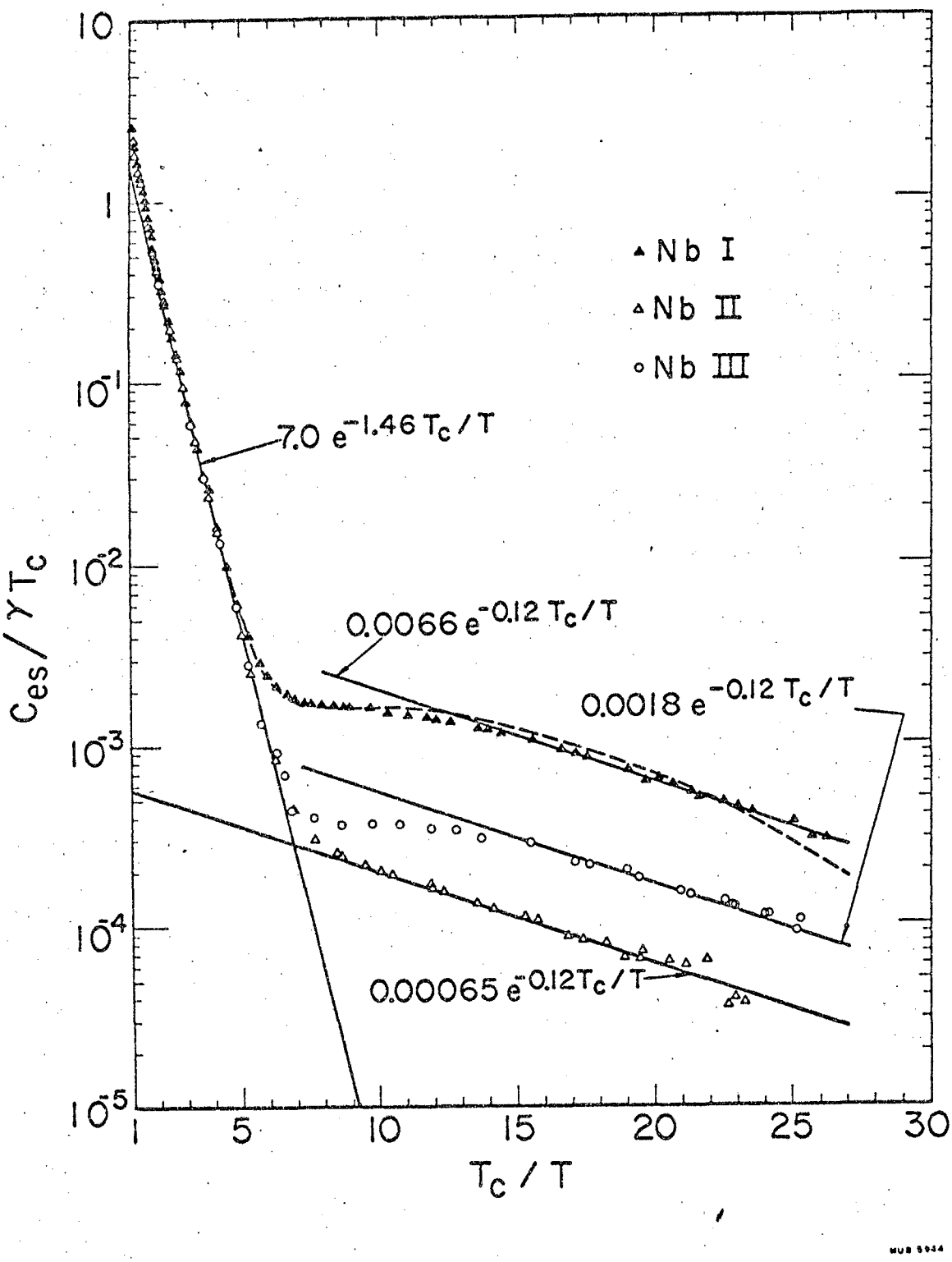

Fig. 11

The superconducting-state electronic heat capacities of different-purity niobium samples. The dashed curve represents the expression $C_{es}/\gamma T_c = 7.0 \exp(-1.46\ T_c/T) + 0.0038\ (0.25\ T_c/T)^2 \exp(0.25\ T_c/T)\ (1 + \exp(0.25\ T_c/T))^{-2}$.

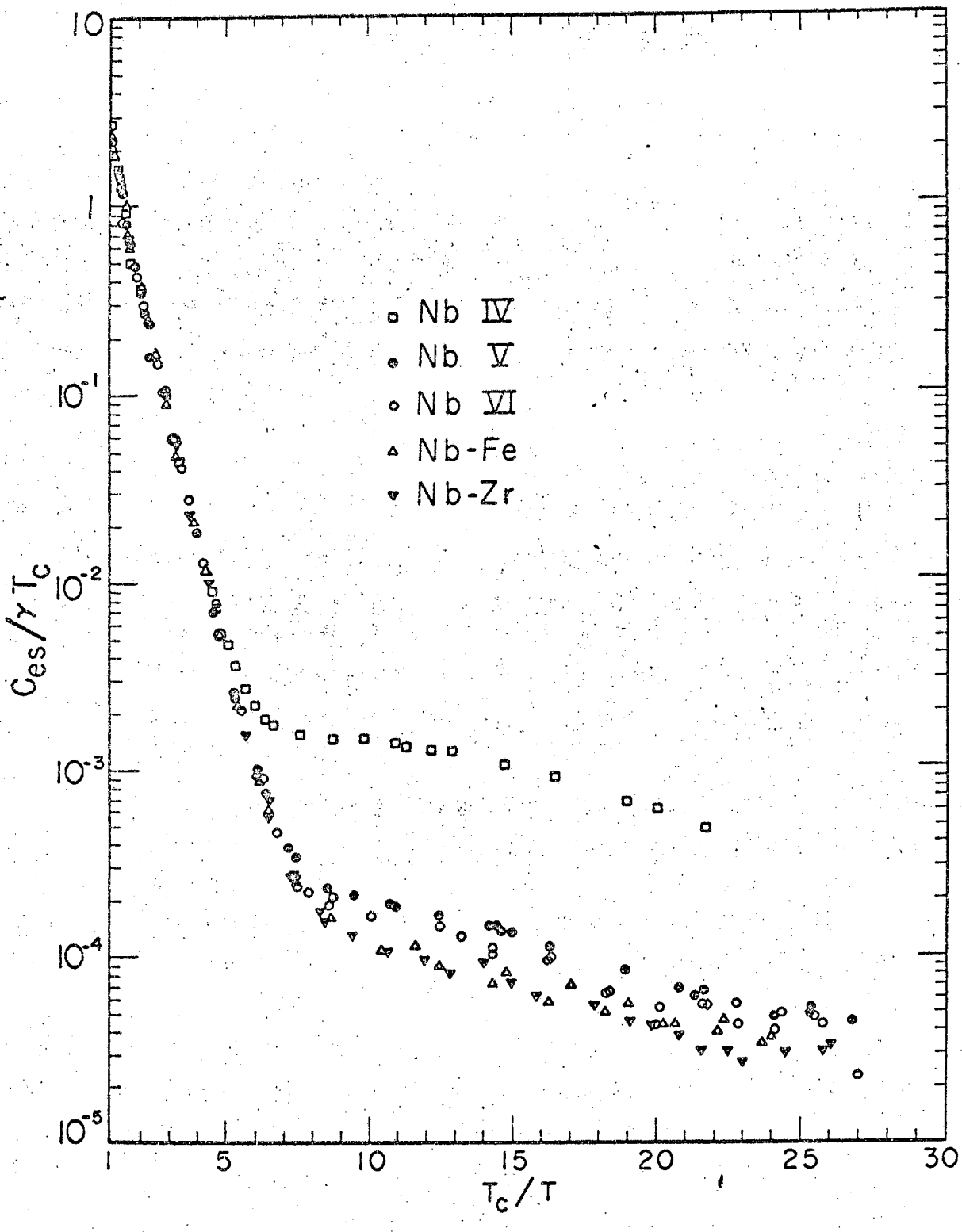

Fig. 12

The superconducting-state electronic heat capacities of NbIV, NbV, NbVI, Nb-Zr and Nb-Fe.

"strong-coupling" effects.[17] D(t) is not sensitive to the anomalous C_s below $T_c/6$. Following Eq. (7) we can determine that the value of the energy gap $2\Delta(0)$ is 3.69 kT_c at 0°K.

3. Tantalum

Three tantalum samples of different impurity contents were used for this experiment. Ta II was a triply zone-refined single crystal that was prepared from the same material as polycrystalline Ta III. Ta I consisted of two zone-refined single crystals that were bound together by a copper foil and a small amount of G.E. 7031 varnish which constituted additional contributions to the addenda. Table VII lists the impurity contents of Ta II and III as given by the supplier. The normal state data below 4.2°K, in a 24 KG field, are represented by

$$C_n = 0.01/T^2 + 6.02\ T + 0.113\ T^3 + 0.00019\ T^5 \quad \text{mJ/mole-°K.}$$

The T^{-2} term was determined by plotting CT^2 vs T^3 for the below 1°K data of Ta III. The nuclear moment of tantalum is small (2.1 nm) relative to that of vanadium and niobium, and hence C_{nuc} is correspondingly small. C_n of Ta I and Ta II are essentially the same as Ta III.

Approximate values of T and T^3 coefficients have been found by plotting C_n/T vs T^2 as shown in Fig. 13. Final values of $\gamma = 6.02$ mJ/mole-°K^2, $\alpha = 0.113$ mJ/mole-°K^4, and $\beta = 0.00019$ mJ/mole-°K^6 have been obtained by plotting $(C_n - \gamma T)/T^3$ vs T^2 for different γ's in Fig. 14. A different value of γ can greatly distort the expected linear behavior of the experimental points.

Figure 15 shows the heat capacities taken with small temperature increments (about 5 millidegrees) near T_c. T_c is equal to 4.478°K for Ta I, 4.455°K for Ta II and 4.450°K for Ta III. The difference in heat capacities between the normal and superconducting states, $(C_s - C_n)/\gamma T_c$, is best determined to be 1.51 for Ta II at T_c. Table VIII shows the results for different tantalum samples.

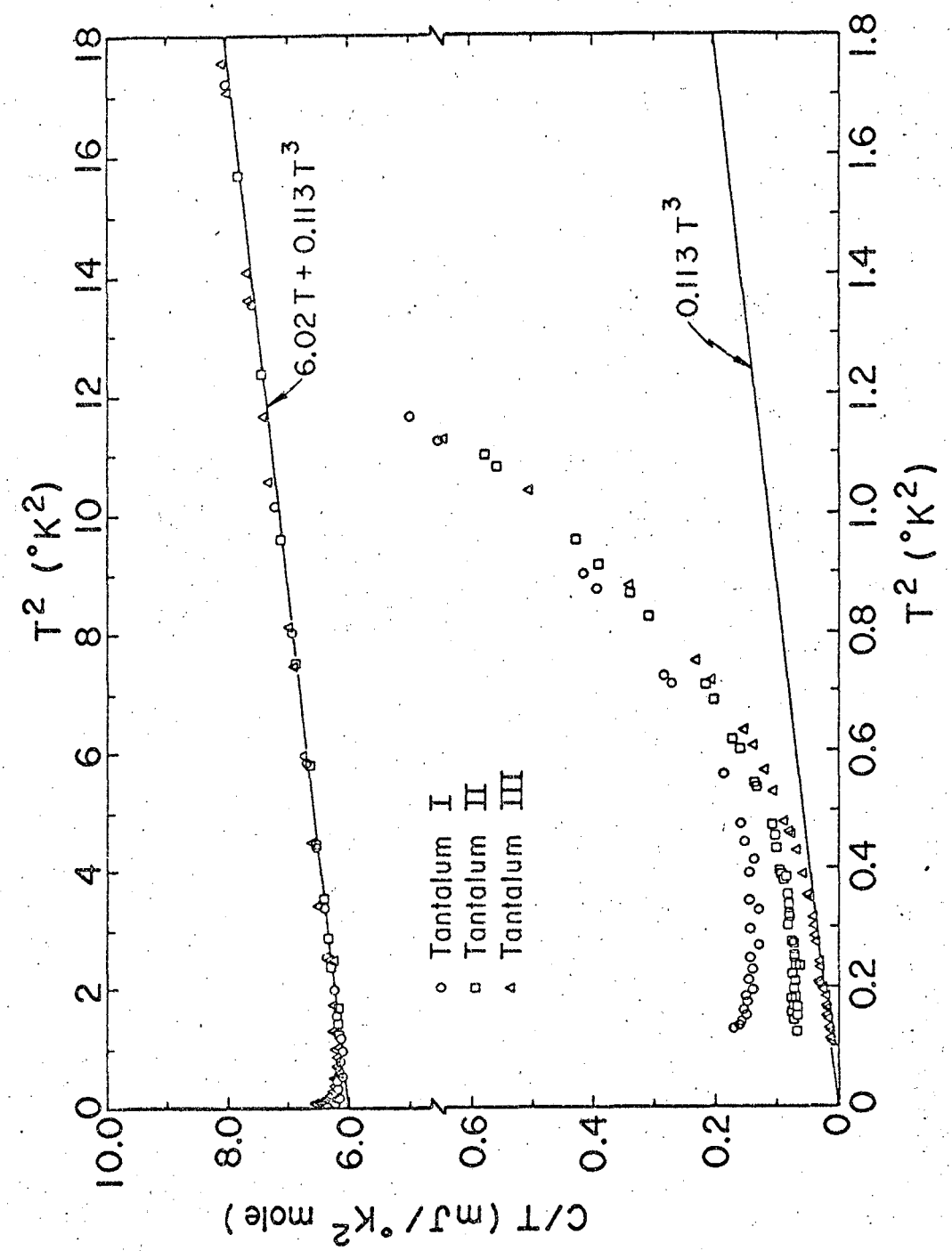

Fig. 13

The heat capacities of different-purity tantalum samples. The slopes of the solid lines represent $C_{\ell n}$.

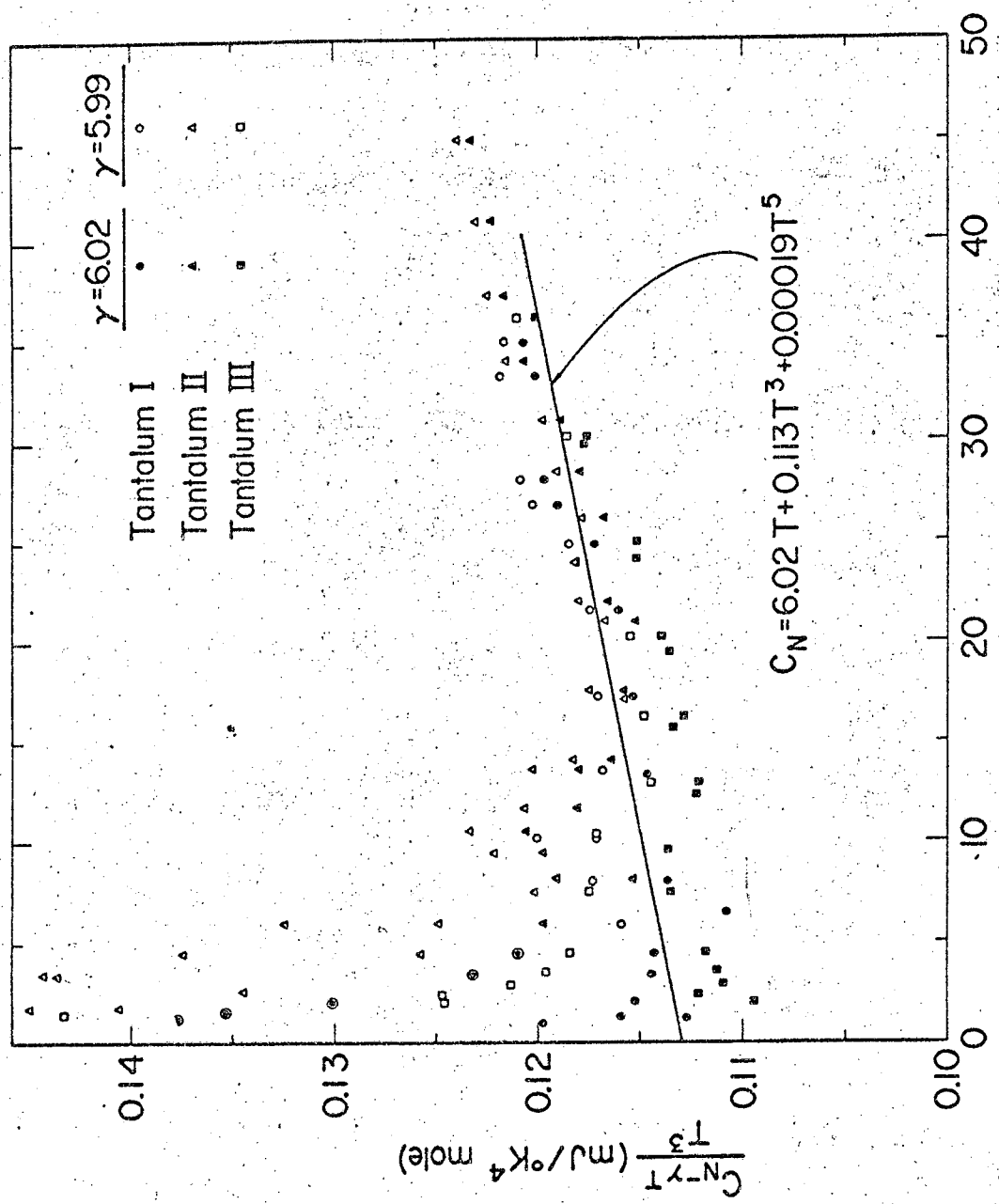

Fig. 14

The lattice heat capacity of normal tantalum.

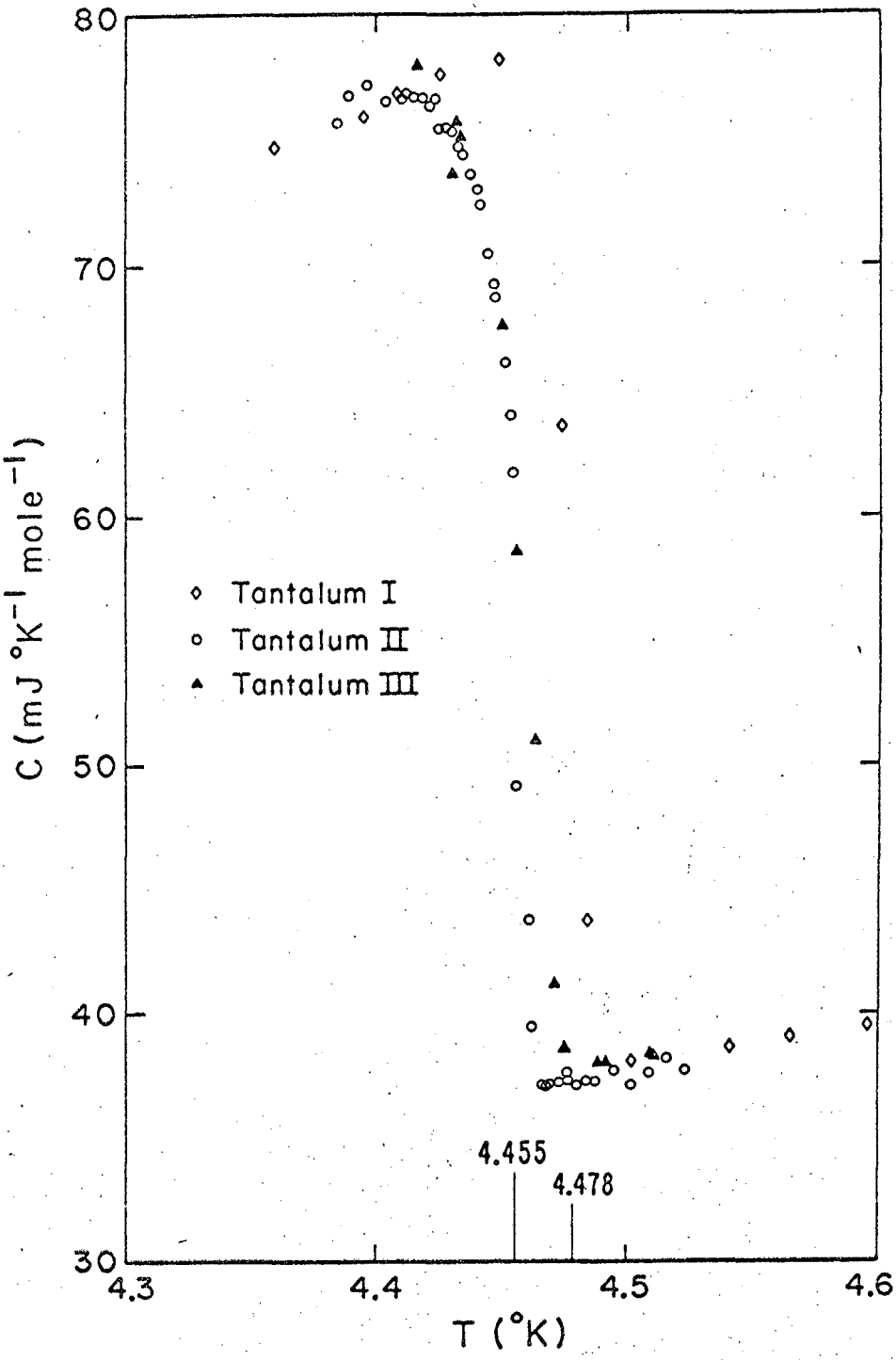

Fig. 15.

The heat capacities of three tantalum samples near the transition temperature.

Below 1°K, C_s is plotted in Fig. 13 together with a straight line that represents $C_{\ell n}$. At low temperatures, Ta III is the only case for which C_s approaches $C_{\ell n}$. C_s of high-purity tantalum is similar to that of niobium where it behaves anomalously for $T < T_c/6$. Figure 16 shows $C_{es}/\gamma T_c$ on a semi-logrithmatic graph, where $C_{es} = C_s - 0.113\ T^3 - 0.00019\ T^5$. Between $T_c/2$ and $T_c/6$, C_{es} is the same for the three samples and is represented by $C_{es}/\gamma T_c = 8.13 \exp(-1.45 T_c/T)$. The exponent is equivalent to the energy gap $2\Delta(0) = 3.55\ kT_c$. Below $T_c/6$, excess C_{es} appears in pure tantalum. Although the measurements extend only to $T = T_c/13$, the nearly temperature-independent C_{es} between $T_c/8$ and $T_c/13$ seems to be the common property of high-purity niobium and tantalum.

We calculated $H_c(T)$ from the smoothed values of C_s and C_n of Ta II according to Eq. (6). For this purpose, T_c was taken to be 4.442°K at which the entropy difference vanished. The uncertainty in the extrapolation of C_s/T to T = 0°K was not significant. $V_m = 10.82\ cm^3/mole$ has been estimated from the known lattice parameters of tantalum.[11] $H_c(0)$ has been found to be 814 G. Figure 8 shows the plot of D(t) vs t^2 for Ta II. Following Eq. (7), the value of $2\Delta(0)$ is determined as $3.55\ kT_c$ from the experimental values of $H_c(0)$, γ, and T_c. Table IX summarizes the comparison of our data with other related measurements on tantalum.

The value of the energy gap can be obtained by different methods. A complete list of $2\Delta(0)$, together with our measurement, is presented in Table X for vanadium, niobium, and tantalum.

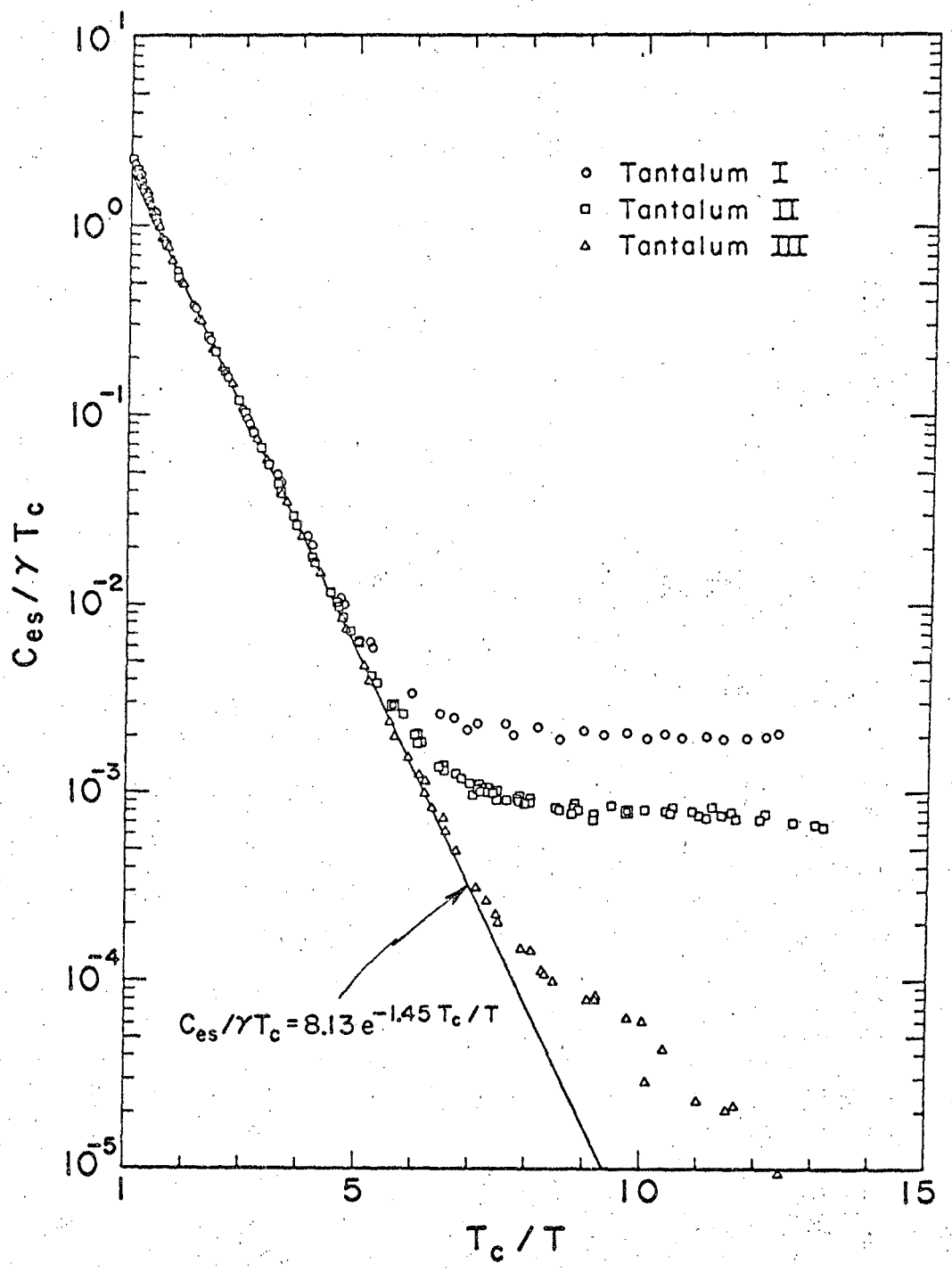

Fig. 16

The superconducting-state electronic heat capacities of different-purity tantalum samples.

D. DISCUSSION

1. Mean-free-path Effect on Transition Temperature

For concentrations of non-magnetic impurities, of the order of a few tenths of an atomic percent, T_c decreases linearly with the reciprocal electronic mean free path ℓ. This effect was first pointed out by Lynton, Serin, and Zucker[18] on a purely experimental basis. Anderson[19] later showed that a smearing-out of the energy gap anisotropy by the impurities could lead to this effect. When the lowering of T_c by impurities is dominated by the reduction in energy gap anisotropy, it is determined entirely by $1/\ell$, and is independent of the nature of the impurities. According to the more detailed theory of Markowitz and Kadanoff[20] the impurities have two effects on T_c: (1) the gross properties of the system are changed by the impurities and produce a linear change in T_c -- the valence effect, and (2) the anisotropy of the energy gap is reduced by impurity scattering and produces an abrupt initial decrease in T_c -- the mean-free-path effect. At the limit of low impurity concentrations, where the coherence length ξ is less than ℓ, both effects are linear with respect to $1/\ell$, i.e., proportional to the residual resistance $\rho = R_{4.2}/R_{300}$. In this region, the valence effect is small compared with the mean-free-path effect for the metals that have been studied.

In our measurements, T_c is taken to be the midpoint of the heat capacity jump, and therefore truly represents a bulk property. Figure 17 shows the result on the niobium samples. Our results show that T_c decreases linearly with ρ. The extrapolated T_c in the pure sample limit is 9.294°K for

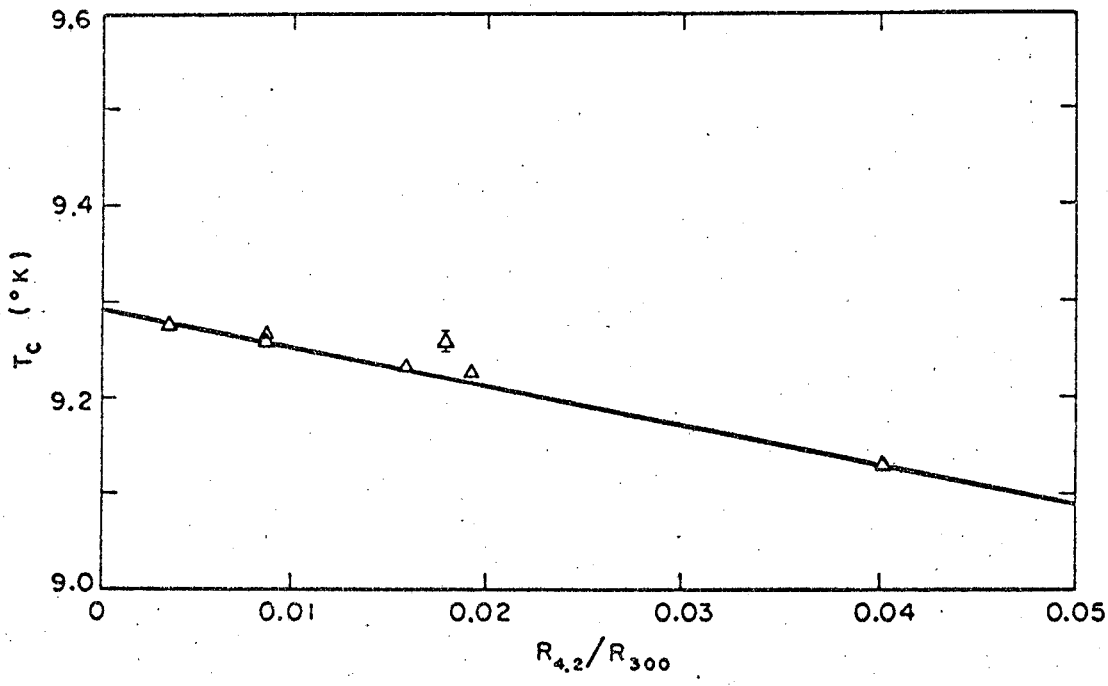

Fig. 17

The change of transition temperature vs the reciprocal of the residual resistance for niobium.

niobium. The slope $\Delta T_c/\rho$ of the straight line is -4.1°K.

Figure 17 shows the T_c vs ρ plot for tantalum. Our data fall on the straight line that was reproted by Budnick[22] as the best representation of his points over a wider range of ρ. The extrapolated T_c in the pure sample limit is 4.485°K for tantalum, and the slope of the line is $\Delta T_c/\rho = -2.56$°K.

Since our samples contain a variety of impurities and the points in each of Figs. 16 and 17 are linear in ρ, we can conclude that the lowering of T_c is dominated by the smearing-out of the energy gap anisotropy. Consequently, the effects of anisotropy on the thermodynamic properties of our samples are likely to be found. In the low-impurity region, where $\xi \ll \ell$, the theory of Markowitz and Kadanoff[20] gives the following relation:

$$\frac{\Delta T_c}{T_c} = -\frac{\pi}{8}\,\frac{\xi_o}{0.18\ell}\,\langle a^2\rangle \qquad (8)$$

Where the energy gap anisotropy is expressed by means of multiplying the BCS energy gap by $(1 + a(\Omega))$ -- an angle-dependent factor for which $\langle a\rangle = 0$. In order to obtain the value of $\langle a^2\rangle$, we need to know the ratio ξ_o/ℓ which is proportional to the area of the Fermi surface obtained usually from the anomalous skin effect. This information is not available for niobium and tantalum, but in the case of niobium ξ_o could be found from the ratio of London penetration depth and the Ginzburg-Landau parameter. The former was measured to be 3.9×10^{-6} cm by Maxfield and Mclean,[21] the latter was reported to be 1.1 by Stromberg and Swenson.[16] Hence, $\xi_o \sim 3.6 \times 10^{-6}$ cm and from that, the Fermi velocity $v_F \sim 2.6 \times 10^7$ cm/sec was calculated from the BCS relation.[2] Making

use of a free electron model and this value of Fermi velocity which corresponds to a Fermi surface which is 1/3 of the free electron value with 5 electrons per atom, the ratio ξ_o/ℓ has been found approximately equal to 3.0ρ[37] for niobium. For our dirtiest niobium, $\ell \simeq 0.31 \times 10^{-4}$ cm which is larger than ξ, hence Eq. (8) is valid to represent our data. $\langle a^2 \rangle$ has been found to be 0.07 for niobium.

In the case of tantalum we could estimate the area of the Fermi surface to be close to that of niobium by analogy with what Fawcett[23] found for W, and Mo. This is equivalent to using the same v_F for both Nb and Ta. The ratio ξ_o/ℓ is then found to be approximately 6.6ρ. For our dirtiest tantalum $\ell \simeq 8.9 \times 10^{-5}$ cm which is larger than $\xi \simeq \xi_o \simeq 8.1 \times 10^{-6}$ cm, hence Eq. (8) could be used. $\langle a^2 \rangle$ has been determined as 0.04.

A comparison of $\langle a^2 \rangle$ for niobium and tantalum with the values for some non-transition metals is presented in the following table.

	$\langle a^2 \rangle$
Al[20]	0.001
In[20]	0.019
Sn[20]	0.021
Nb	0.07
Ta	0.04

The above estimation of the energy gap anisotropy in terms of $\langle a^2 \rangle$ is based on the use of the theory of Markowitz and Kadanoff,[20] the BCS relation $\xi_o = 0.18 \frac{\hbar}{k} \frac{v_F}{T_c}^2$, and the estimation of the Fermi surface area

which is proportional to v_F^2 for a free electron model. In the present cases where there might exist two distinct energy gaps (see Sec. 4) the meaning of Eq. (8) is less clear than implied in its original derivation.

2. Nuclear Heat Capacity

We have observed, for the first time, the effect of an external magnetic field on the heat capacity of nuclei. The observed T^{-2} terms in C_n were , in all cases, consistent with the known nuclear moments and the average of H^2 over the volume of the sample. Experimentally, $\langle H^2 \rangle$ depended on the position of the sample relative to that of the superconducting magnet, and was not determined to better than 10%. The large contribution from C_{nuc}, however, limited the accurate determination of γ and θ_o in the normal state below 0.8°K. If we reduce the external field to the point that C_{nuc} is negligible, a small fraction of the sample becomes superconducting, and adds an unknown amount to the measured heat capacity.

The determination of C_{nuc} contains no new information apart from the fact that the nuclear-lattice relaxation time is short enough that the heat capacity of the nuclei could be observed.

3. Lattice Heat Capacity

In the normal state, the lattice heat capacity was analyzed graphically based on Eq. (1). A least squares fit by computer was also made with essentially the same result. Below 1°K the lattice heat capacity is a small fraction of the total heat capacity, which includes the large electronic term characteristic of the transition metals. For this reason, and because of the T^{-2} term, we give more weight to measurements between 1 and 4°K in determining Θ_0. The effect of the impurities on $C_{\ell n}$ is negligible, although the limitation on the accuracy of our determination should be kept in mind.

The Debye characteristic temperature Θ_e which is calculated from elastic constants[3] lies within the error limit of Θ_0 which is obtained by extrapolating $C_{\ell n}$ from higher temperatures for vanadium and niobium. No comparison can be made for tantalum because the elastic constants at 4°K are not available.

The observed low-temperature C_s cannot be expressed simply as the sum of αT^3 and the BCS expression for C_{es}.[2] The discrepancy is especially pronounced for high-purity niobium and tantalum, of which C_s's have a very complicated temperature dependence. Therefore, it is necessary to consider the possible causes for this behavior.

The possibility of "frozen-in-flux" existing in the superconducting samples can be ruled out. The reasons are as follows. First, the samples were cooled to 0.3°K in 1/30 of the earth's field, and the superconducting-state measurements always preceded the normal-state measurements. Second, during the Ta II run, it was observed that C_s measured in the earth's field was the same as in zero-field. This indicated that, even if a small stray magnetic field existed, the sample expelled it completely (Meissner effect).

Third, the application and the removal of a strong magnetic field during the Ta II run produced an additional heat capacity that was equal to 0.1xT mJ/mole-°K, as expected from "frozen-in-flux", whereas the observed anomalous heat capacity was not linear in T. Hence, we believe that no "frozen-in-flux" exists in our superconducting-state measurements.

For a few non-transition-metal superconductors, there have been heat capacity measurements that gave information about $C_{\ell s}$. Tin,[4] mercury,[24] and thallium,[25] all give the expected result, $C_{\ell s} = C_{\ell n}$. A small discrepancy (proportional to T^3) has been reported for lead,[26] but measurements by W. R. Gardner in this laboratory[24] showed no such discrepancy. Only for indium[4] does it seem possible that there is a discrepancy, and in this case $C_{\ell s}$ is proportional to T^3 but about 15% smaller than the apparent $C_{\ell n}$. There is no experimental evidence for an anomaly in $C_{\ell n}$ that would explain the C_s observed for vanadium, niobium, and tantalum.

As will be discussed in the following section, for pure transition metals there are theoretical reasons for expecting an excess C_{es} over the BCS value, that can be decreased by the addition of impurities.[19] Since this is in general the kind of behavior observed for vanadium, niobium and tantalum, we conclude that this effect is the important one and that C_s becomes equal to $C_{\ell s}$ at low temperatures only in the "dirty sample" limit. Looking back to our results, we conclude that $C_{\ell s}$ cannot be accurately determined because C_{es} does not become negligible for the lowest-temperature measurements. However, in the cases of "dirty" vanadium and tantalum, C_s approaches $C_{\ell n}$ very closely as shown in Figs. 4 and 12. In fact, a very small discrepancy remains as

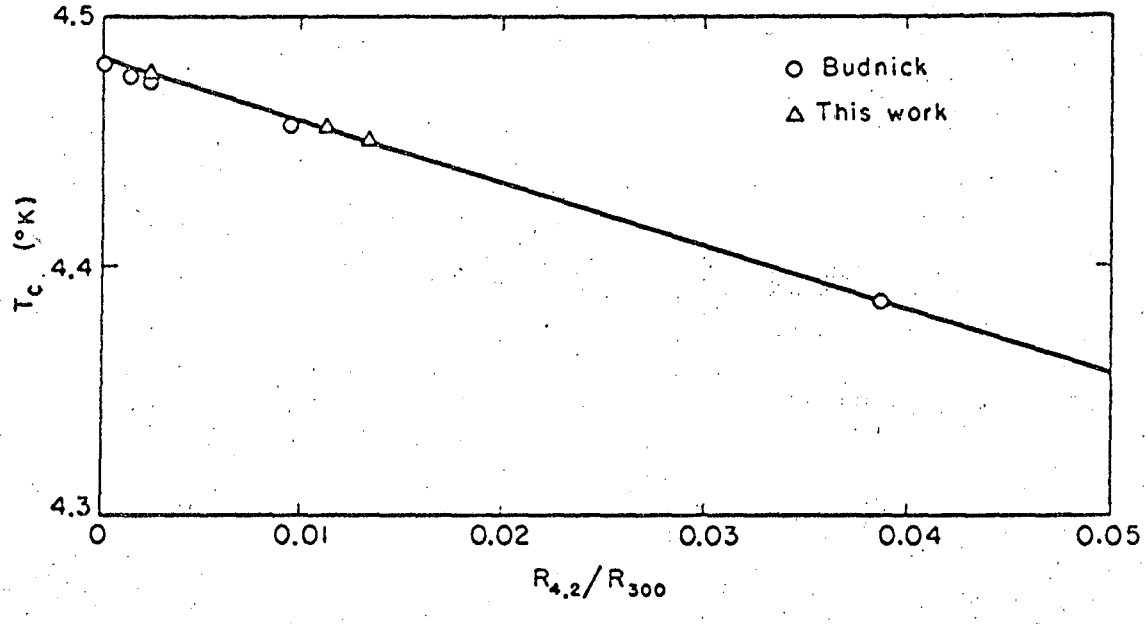

Fig. 18

The change of transition temperature vs the reciprocal of the residual resistance for tantalum. The straight line is taken from Budnick's work.

demonstrated by Figs. 6 and 15. In the case of niobium, C_s is always appreciably larger than $C_{\ell n}$ even in the dirty samples that we studied. Nb II, shown in Fig. 9, is typical. Probably Nb differs from V or Ta in this respect because ξ_o is smaller (about 2.5×10^{-6} cm) for Nb, and the extreme "dirty condition" $\ell \ll \xi_o$ was not reached. The discrepancies between C_s and $C_{\ell n}$ for the "dirty" niobium samples are very different in magnitude, sign, and temperature dependence from the apparent discrepancy between $C_{\ell s}$ and $C_{\ell n}$ for indium.[4] Therefore, there is more reason to believe that C_{es} behaves anomalously than there is to believe that $C_{\ell s} \neq C_{\ell n}$. We conclude from the present evidence that $C_{\ell s}$ cannot differ very much from $C_{\ell n}$, and is very likely to be equal. Certainly, there is no discrepancy like that of indium, as reported by Hirshfeld, Leupold and Boorse.[27]

The equalities of Θ_o and Θ_e and of $C_{\ell n}$ and $C_{\ell s}$, agree with other measurements on a majority of pure metals. They thus do not support the recent theory of Eliashberg[1] who proposed that the lattice heat capacity of the normal state is proportional to $T^3 \log T$, and that $C_{\ell s} \neq C_{\ell n}$.

In general, our niobium results for "dirty" samples, agree with recent reports by Van der Hoeven and Keesom,[28] and by Leupold and Boorse[14] above 0.7°K. We note that Keesom et al[28] attributed the excess heat capacity of the superconducting niobium to strains or impurities instead of the anisotropic effect.

The high-temperature normal-state heat capacities for vanadium and tantalum are plotted in terms of Θ vs T, where Θ is defined in Eq. (1). The corresponding plot for niobium was given by Senozan.[8] Figures 19 and 20 indicate that Θ has the usual kind of temperature dependence for vanadium and tantalum. A similar curvature was also found in niobium.

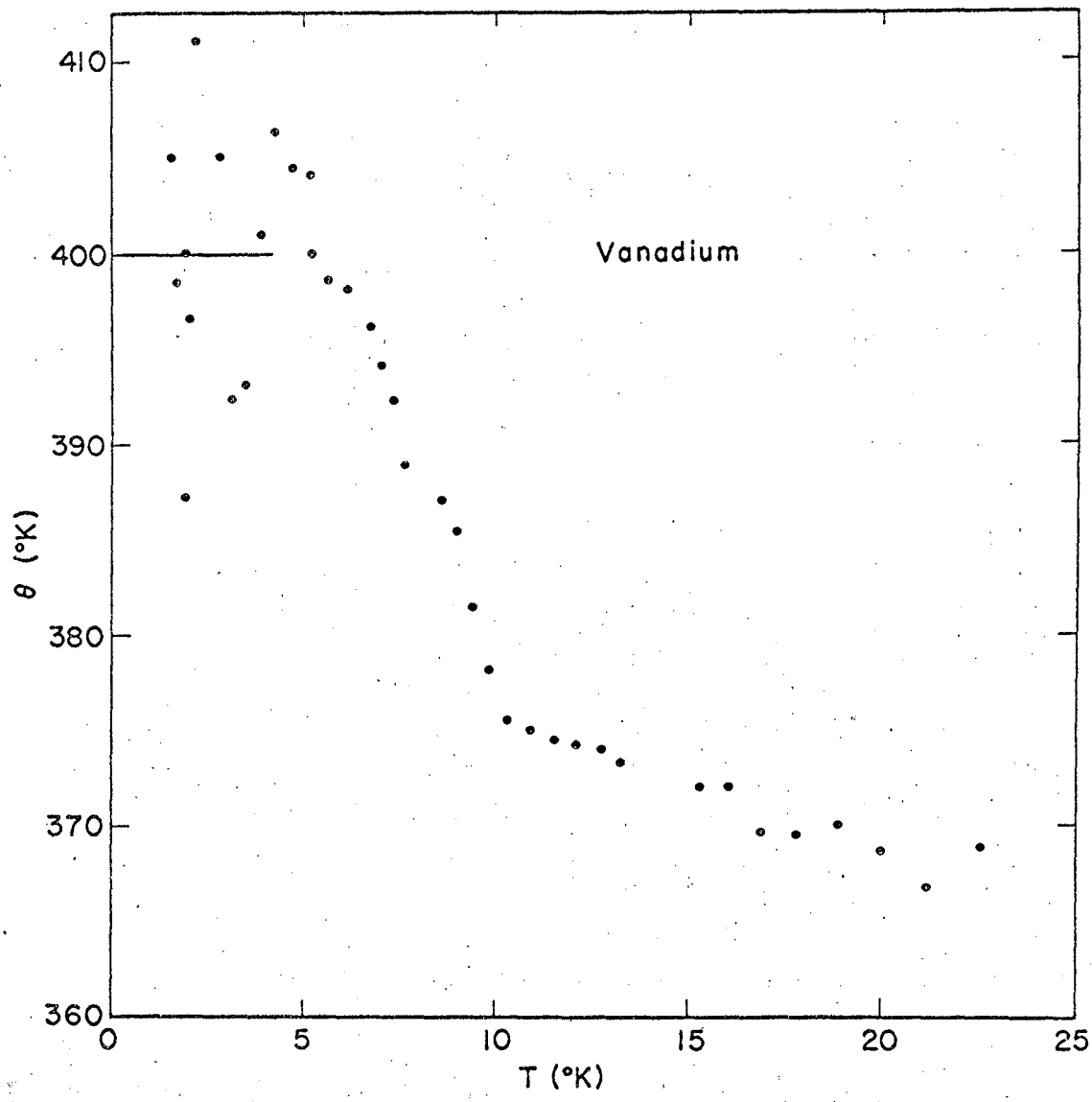

Fig. 19

Variation of the Debye temperature of vanadium with temperature.

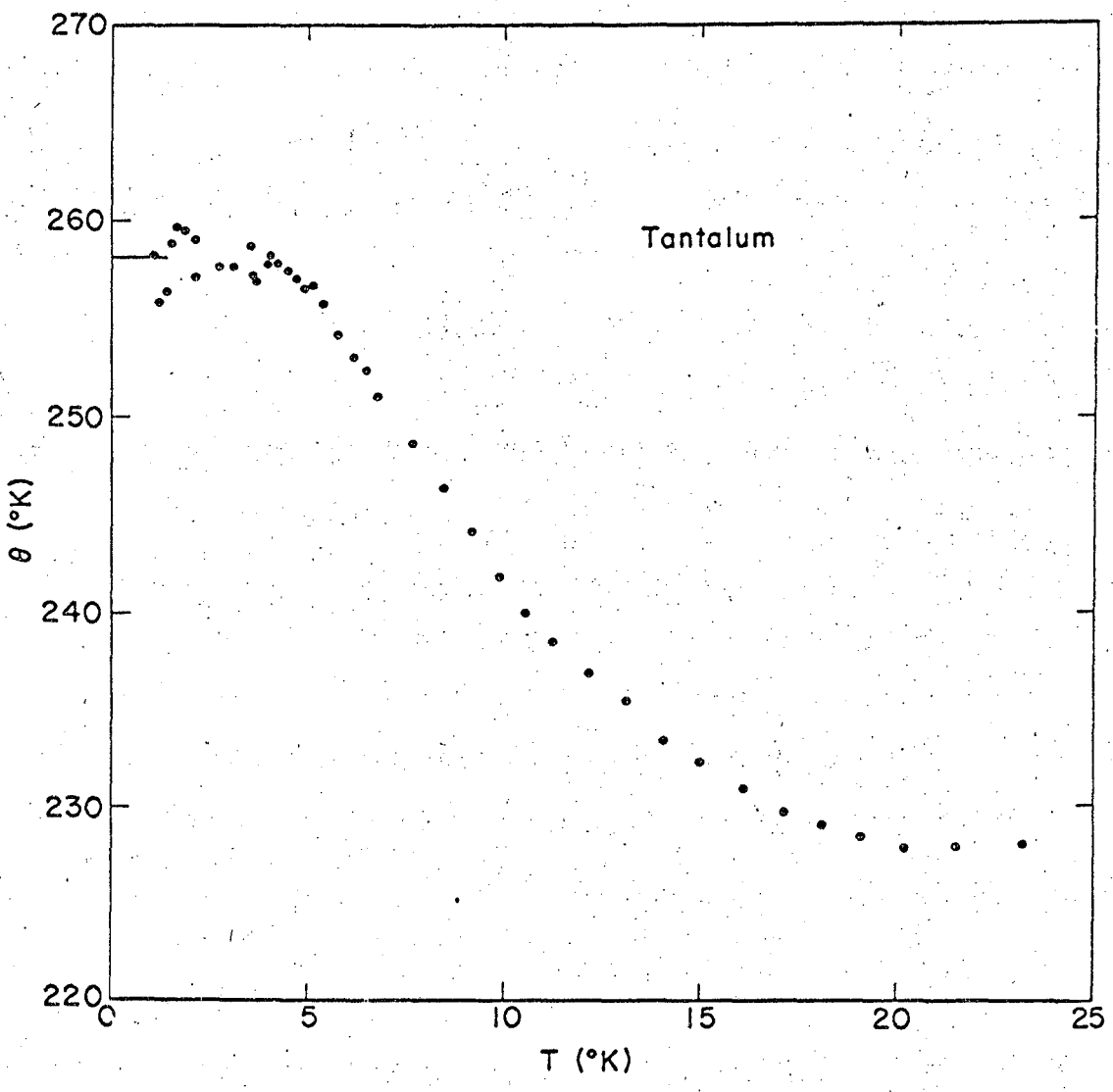

Fig. 20

Variation of the Debye temperature of tantalum with temperature.

4. Electronic Heat Capacity

a. Heat Capacity Discontinuities at the Transition Temperature

Near T_c the BCS theory predicts a finite heat capacity discontinuity, $(C_s-C_n)/\gamma T_c = 1.43$. Experimental values are either equal to or slightly higher than 1.43. Teh observed magnitude of this ratio is related to T_c/Θ_o, and is a measure of the "strong coupling" effect. Present determinations of $(C_s-C_n)/\gamma T_c$ are listed in Tables III, VI, and VIII. The averaged values of $(C_s-C_n)/\gamma T_c$ of different metals follows the general behavior of various superconductors.[29] The small variations of $(C_s-C_n)/\gamma T_c$ from sample to sample are probably related to the energy gap anisotropy.[30]

b. Qualitative Features of the Electronic Heat Capacities at Low Temperatures

The superconducting-state heat capacity of high-purity V, Nb, and Ta below $T_c/6$ is considerably different from previously reported measurements.[14,28,31] Few measurements of C_{es} on metals extend to reduced temperatures low enough to compare with our data. Some of the early measurements below 1°K showed positive deviations from exponential behavior at the lowest temperature reached, but different measurements on the same metals did not agree. Tin, for which deviations had been reported, is one of the most favorable examples for experimental investigation (high Θ_o and T_c), and two recent measurements[4,32] on high-purity samples agree in showing a simple exponential temperature dependence of C_{es} down to $T \sim T_c/9$, below which C_{es} is lost in the lattice heat capacity. The energy-gap anisotropy that has been observed by more direct methods in V, Nb, and Ta, is far too small (about 10%) to account for the two exponential terms in C_{es} of Nb. Both V and Ta show behavior similar to that of Nb of corresponding purity (but the measurements extend only to

$T \sim T_c/12$). As a function of reduced temperature $t = T/T_c$, $C_{es}/\gamma T_c$ is strikingly similar for all three metals. This suggests that a simplified model may be useful, in spite of the complexity of the electronic structure of these metals.[33]

Suhl, Matthias, and Walker (SMW)[7] pointed out that transition-metal superconductors might have two distinct energy gaps. In connection with his calculations on the isotope effect in transition metals, Garland[34] suggested that this would produce anomalies in the thermodynamic properties. Our observed C_{es} for the "pure class"niobium samples can be partially explained on the basis of SMW's model. The sensitivity of C_{es} to sample purity can be understood on the basis of Anderson's theory[19] of "dirty" superconductors, and explains why the deviation from a simple exponential has not been observed in earlier measurements. We present in the remainder of this section a qualitative interpretation of the results and in the last section a more quantitative comparison with the SMW's model without introducing the impurity effects.

We shall concentrate on the heat capacity of niobium because a wider range of reduced temperature is available. The sum of two exponentials, which fit both the high temperature region and the low temperature region does not fit the experimental data in the intermediate region. Empirically, a Schottky anomaly -- $0.0038 \frac{(0.25\ T_c/T)^2 \exp(0.25\ T_c/T)}{1 + \exp(0.25\ T_c/T)}$ -- represents $C_{es}/\gamma T_c - 7.0 \exp(-1.46\ T_c/T)$ very well as shown by the dashed curve in Fig. 11. Intuitively one might expect this to give an approximate representation of the anomaly in C_{es} if the second energy gap $\Delta_s(0)$ is independent of temperature at $kT \lesssim \Delta_s(0)$. The coefficient of the exponential in the Schottky curve suggests $\Delta_s(0) \sim 0.25\ kT_c$. We note, however, that the Schottky curve is not a good fit to the lowest temperature points,

and these points alone suggest $\Delta_s(0) \sim 0.12\ kT_c$. The second energy gap $\Delta_s(0)$ determined by different methods is between $0.12\ kT_c$ which differs from the BCS value of $1.76\ kT_c$ by an order of magnitude.

For none of the "dirty" niobium samples that were measured does C_{es} approach the BCS value as closely as the "dirty" tantalum and vanadium. This was probably because the coherence length of Nb was shorter than that of V and Ta, and the "dirty" limit could not be reached without introducing a large amount of impurities. If more than 1% impurities were introduced the lattice heat capacity would probably be affected by impurities thus causing difficulties in the separation of C_{es} and C_s, whereas in the purer samples we could use the limiting value of $C_{\ell s}$ that was calculated accurately from the elastic constants.

c. Relationship between C_{es} and T_c

At first thought, our interpretation leads to a correlation between the anomaly in C_{es} and the value of T_c which is related to the residual resistances in the low-impurity limit. This is indeed the case for the three tantalum samples investigated. To our surprise, the niobium samples did not follow this pattern. Nb III has a higher T_c than Nb I but the low temperature C_{es} of Nb III becomes lower than Nb I. The polycrystalline Nb IV has the same T_c as Nb I but the low temperature C_{es} of Nb VI behaves like Nb II of the "dirty class". To clarify this puzzle, we put Nb IV which belonged to the "clean class" through an annealing process at 1200°C and 10^{-4} mm Hg pressure for 24 hours. The "clean" sample absorbed gaseous impurities during the heating process and $R_{4.2}$ (normal-state) increased by a factor of two. After the treatment, C_{es} at low temperatures decreases by a factor of 10 on the same sample. This phenomena is consistent with the fact that the energy gap anisotropy is smeared out by the addition of

impurities to the sample.

To interpret the incomplete correlation between high T_c and high low-temperature C_{es}, we are forced to accept that an impurity can affect T_c and the low-temperature C_e differently. The ordering parameter, which is a measure of the density of the superconducting electrons, is quite different near T_c and at low temperatures. Hence, the effect of impurities on superconducting electrons could be different at different temperatures, and one particular kind of impurity may affect C_{es} more than T_c. The complexity of the "impurity" problem is revealed by the theory of Markowitz and Kadanoff[20] that gave an expression for the lowering of T_c by impurities. In their theory which was valid near T_c, they introduced a collision time τ_a, characterizing the mean time for smearing-out the energy-gap anisotropy, and a different collision time τ_t, characterizing the residual resistivity ρ. Their analysis of the experimental data of Lynton et al[18] showed that the ratio τ_a/τ_t was different for each impurity in a given host. If we further assumed that τ_a/τ_t depended on temperature, the energy-gap anisotropy could be smeared out in one way near T_c and in another way at lower temperatures. In other words, T_c may not be the only criterion deciding how C_{es} should behave at low temperatures. It is most unfortunate that we cannot control the minute quantity of impurities in niobium which cannot be purified easily.

d. Two Energy Gap Theory at the "Clean Sample" Limit

If we assume that the heat capacity of the "clean" class niobium represents the case where no impurity is present, we can use the SMW model to fit the data in a semi-quantitative way. In view of the complexity of the real situation, this is not the only approach that might explain the results. The extension of this method to the "dirty" case was difficult and produced poor results.

The basic assumption of the two-energy-gap theory is that there exist two distinct energy gaps in superconductors having two energy bands. The two gaps correspond to the possibility of forming pair states for either s- or d- states. The larger gap corresponds to the ordinary BCS energy gap that explains the usual properties of superconductors. At lower temperatures, few quasi-particles have enough thermal energy to jump across the larger energy gap, and the smaller gap becomes important. With this additional degree of freedom, we separate C_{es} into two parts that represent the larger gap Δ_d and the smaller gap Δ_s, respectively. This approximation implies the neglect of the interaction between two types of quasi-particles. The theory is a special model of anisotropic energy gap in which we make use of SMW's Hamiltonian to fit the experimental data. Attention will be concentrated on pure niobium (Nb I) because of the large reduced temperature range covered by the experimental data. No effort was made to fit tantalum data which did not extend to low enough reduced temperatures.

According to the theory, we can determine the following parameters of the two-gap model: the small energy gap Δ_s, N_s/N_d, ($N_{s,(d)}$ is the density of states of s-(d-) band) and the magnitude of the inter-band-interaction J.

The Hamiltonian of a pure two-gap superconductor

$$H = \sum_{k,\sigma} \epsilon_{ks} S^{+}_{k\sigma} S_{k\sigma} + \Sigma\epsilon_{kd} d^{+}_{k\sigma} d_{k\sigma} + J_s \sum_{k,k'} S^{+}_{k\uparrow} S^{+}_{-k\downarrow} S_{k'\downarrow} S_{-k'\uparrow}$$

$$+ J_d \sum_{k,k'} d^{+}_{k\uparrow} d^{+}_{-k\downarrow} d_{k'\downarrow} d_{-k'\uparrow} + J \sum_{k,k'} (S^{+}_{k\uparrow} S^{+}_{-k\downarrow} d_{k'\downarrow} d_{-k'\uparrow} + \text{H.C.}) \quad (9)$$

where ϵ_{ks} and ϵ_{kd} are the s- and d- band kinetic energy measured from the Fermi surface and $S^{+}_{k\sigma}(d^{+}_{k\sigma})$, $S_{k\sigma}$ $(d_{k\sigma})$ are the corresponding creation and annihilation operators. J_s, J_d, and J are the coupling constants of s-s, s-d, and d-d bands. In Eq. 9, the summations of k are extended over values corresponding to the Debye cut-off frequency $\theta = 277°K$, which is chosen to be the same for both bands. The numerical results of the heat capacity are not sensitive to whether different cut-off frequency are used for different bands.

The equations to determine Δ_s, Δ_d and T_c are taken from the work of Dr. C. C. Sung[35]

$$J_d - J\frac{\Delta_d(T)}{\Delta_s(T)} / N_s\,(J_sJ_d - J^2) = \ell n\,\frac{\Theta}{\Delta_s(T)} - 2\sum_{n=0}^{\infty}(-1)^n\,K_o\left[(n+1)\frac{\Delta_s(T)}{T}\right] \quad (10)$$

$$J_s - J\frac{\Delta_s(T)}{\Delta_d(T)} / N_d\,(J_sJ_d - J^2) = \ell n\,\frac{\Theta}{\Delta_d(T)} - 2\sum_{n=0}^{\infty}(-1)^n\,K_o\left[(n+1)\frac{\Delta_d(T)}{T}\right] \quad (11)$$

$$W^2(J_sJ_d - J^2)\,N_sN_d + (J_sN_s + J_dN_d)\,W + 1 = 0 \quad (12)$$

where $W = \ell n\,(0.88\,T_c/\Theta)$ and K_n is the modified Bessel function of n-th order. We neglect the interactions between the quasi-particles in our model, and write total entropy as the sum of the entropies of s- and d- quasi-particles. It follows that the electronic heat capacity contains two terms:

$$C_{es} = \frac{N_d}{N_s+N_d}\,C^{d}_{es} + \frac{N_s}{N_s+N_d}\,C^{s}_{es} \quad (13)$$

where

$$C^{d}_{es}/\gamma T_c = \frac{N_d}{N_s+N_d}\,\frac{3}{(2\pi)^2}\left(\frac{\Delta_d(T)}{T}\right)^3\frac{T_c^2}{T}\Big\{\sum(-1)^n(n+1)\Big[K_3(u_d(n)) + 3K_1(u_d(n)) + 4\,\frac{d\Delta_d(T)}{d(1/T)}\,\frac{1}{T\Delta_d(T)}\,K_1(u_d(n))\Big]\Big\} \quad (14)$$

$$u_d(n) = (n+1)\,\frac{\Delta_d(T)}{T} \text{ and } \gamma = \frac{2}{3}\,\pi^2(N_s+N_d)\times(\text{Boltzman Constant})^2$$

By exchanging the label (s) and (d) in Eq. (14) we obtain C_{es}^{d}. Which energy gap, Δ_s or Δ_d is larger is determined as follows: since $\frac{N_d}{N_s+N_d} \tilde{=} 1$ and $\frac{N_s}{N_s+N_d} \ll 1$,[36] Δ_d has to be assigned as the larger gap so that at high reduced temperature Eq. (13) gives $C_{es} \tilde{=} C_{es}^{d}$ which fits the experimental data. $\frac{N_s}{N_s+N_d} C_{es}^{s}$ becomes dominant in the low temperature region where

$$T \ll \Delta_d$$

Let $x(T) = \frac{\Delta_s(0)}{\Delta_s(T)}$ and $\alpha = -\frac{\Delta_d(0)}{\Delta_s(0)} \cdot \frac{J}{(N_s N_d - J^2)}$.

Equation (10) becomes

$$2\sum_{n=0}^{\infty} (-1)^n K_o[(u_s(n)] = \ell n\, x(T) - \alpha(1-x) \qquad (15)$$

and

$$\frac{d\Delta_s(T)}{d(\frac{1}{T})} \frac{1}{T\Delta_s(T)} = \frac{2u_s(0) \sum_{n=0}^{\infty} (-1)^n (n+1) K_1(u_s(n))}{1 \alpha x - 2u_s(0) \sum_{n=0}^{\infty} (-1)^n (n+1) K_1(u_s(n))} \qquad (16)$$

Parameters used in determining C_{es}^{s} are N_s/N_d, α, and Δ_s. Equation (15) is solved numerically for x and substituted in Eq. (16) to obtain C_{es}^{s}. $\Delta_s(0)$ is related to the limiting slope of the electronic heat capacity at low temperature limit. The best fit is given by $\Delta_s = 0.16\, T_c$ as shown in Fig.21. In the temperature region $t=T/T_c$ from 0.14 to 0.1, the peculiar temperature dependence of Δ_s accounts for the nearly constant heat capacity. See Fig. 21. α, which is related to the interband coupling constant J, is an important parameter in this region. Finally using $N_s/N_d = 1.5\times10^{-2}$ and adding C_{es}^{s} to C_{es}^{d} we obtain the solid curve shown in Fig. 21.

We note that the parameter to measure the strength of the interband

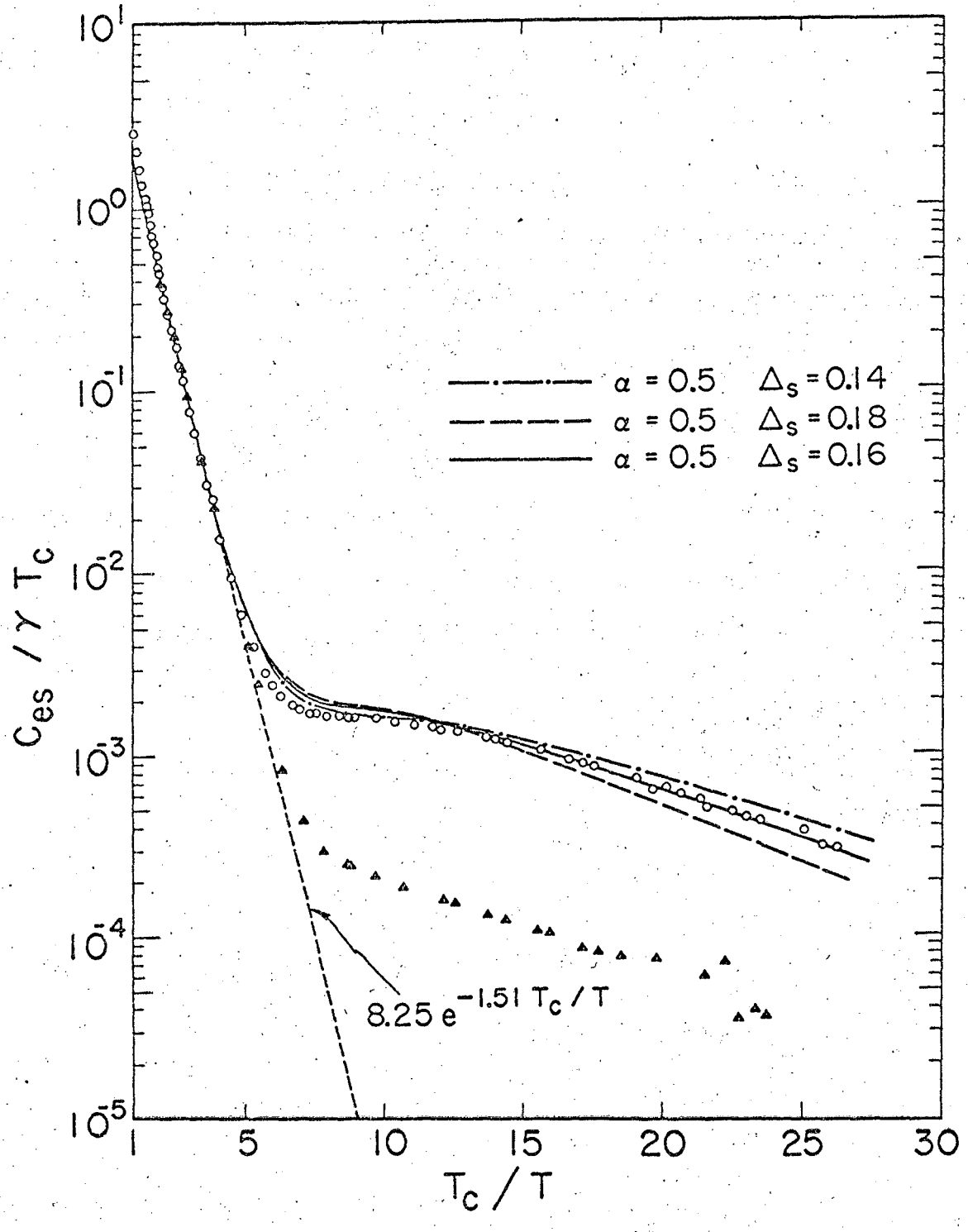

Fig. 21

MUB-7091

The calculation of the superconducting electronic heat capacity for different $\Delta_s(0)$'s based on Eq.(13). The points are the experimental data of Nb I and Nb II.

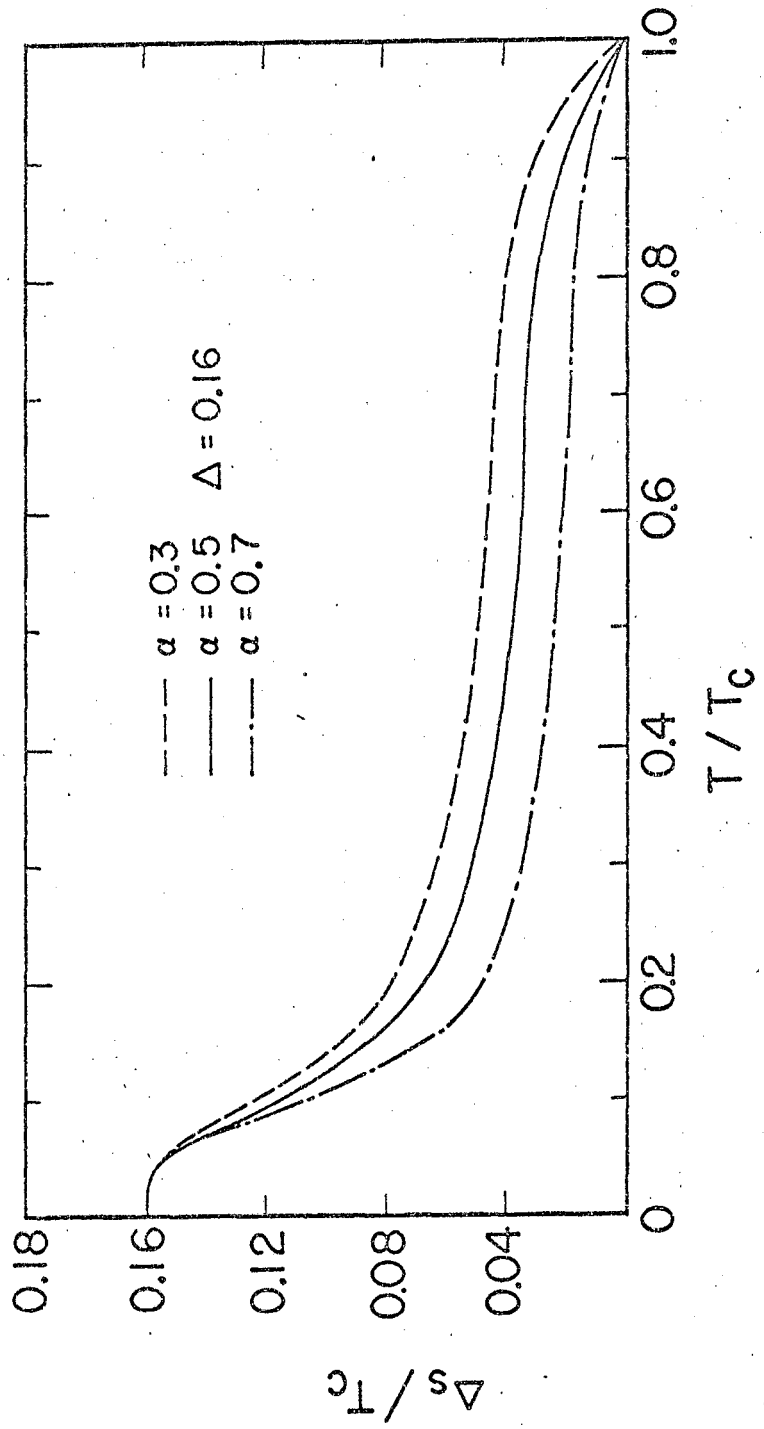

Fig. 22

The value of $\Delta_s(T)$. The change of α between 0.3 and 0.7 does not affect the general feature of the fit with experimental data.

coupling

$$\frac{J(N_s N_d)^{1/2}}{J_s N_s J_d N_d} = \alpha \left(\frac{N_s}{N_d}\right)^{1/2} \sim 0.06.$$

From the parameters Δ_s, Δ_d, and N_s/N_d, which are determined by fitting the data and Eqs. (10-12) we should be able to calculate J_d, J_s and J. However, because of the small values of N_s/N_d and Δ_s/Δ_d and the large experimental uncertainty of T_c and Δ_d we are unable to obtain reliable values of J_d, J_s and J.

The above model gives a reasonable heat capacity of "pure" niobium over the whole measured temperature range. Even though detailed band structure calculations are lacking in niobium, we obtain N_s/N_d from heat capacities alone. The discrepancy with the experimental values and the calculation may be due to (1) the "pure class" is not 100% pure as it is assumed in the calculation and (2) the real physical situation is more complicated than that represented by Eq. (9).

The largest deviation from the experimental data occurred in the region $0.1 > t > 0.14$, where the empirical Schottky formula gave a good fit. A variation in either α or Δ_s could not remove this discrepancy, which limited our ability to determine the parameters other than N_s/N_d and Δ_s. The ratio $N_s/N_d \sim 0.02$ is typical for transition metals and $\Delta_s(0)$ is smaller than the BCS energy gap by an order of magnitude.

A more refined theory would give an extension to the impure case whereas in the present case the attempt was a failure. The present calculation therefore leaves a great deal unexplained.

E. CONCLUSION AND FURTHER SUGGESTIONS

Our observations show that the measurements of heat capacities of superconductors can be used to study the nature of the energy-gap anisotropy and its dependence on impurity scattering of superconducting electrons. A two-energy-gap model partially explains the behavior of superconducting heat capacities as a characteristic of transition metals with two energy bands. The observed anisotropy is an order of magnitude larger than that detected in other metals by more direct methods (electron tunnelling, infrared absorption, and ultrasonic wave attenuation).

It would be interesting to study the energy gap anisotropy in niobium by other methods such as microwave absorption and electron tunnelling. The excess contribution to the entropy at low temperatures suggests that there must be an effect on the high-temperature, superconducting-state heat capacity. For niobium and tantalum this effect is too small to be observed but for other transition metals this might not be the case. Another suggestion is to measure the heat capacity of lead-bismuth alloy of a certain composition which has two energy gaps due to "proximity effect". A Pb_{45}-Bi_{55} sample, that was kindly provided by Dr. J. M. Rowell of Bell Telephone Laboratories, has no anomalous heat capacity. Only further studies on the energy gap of high-purity niobium by different methods may be possible to explain the peculiar behavior of the low temperature heat capacity in more detail.

Table I Sample List

	Amount (mole)	$R_{300}/R_{4.2}$	Source	Purity	Physical Form
Vanadium I	1.48	13.3	Material Research Corp.	99.95%	Zone-refined single crystal
Vanadium II	1.38	-	Material Research Corp.	99.95%	Zone-refined single crystal
Niobium I	1.23	110	Material Research Corp.	99.992%	Triply zone-refined single crystal
Niobium II	1.21	24	Union Carbide	99.9%	Polycrystal
Niobium III	0.50	279	Westinghouse Research Laboratories	-	Zone-refined single crystal
Niobium IV	1.25	110	Material Research Corp.	99.95%	Triply zone-refined single crystal
Niobium V	1.25	61.6	Material Research Corp.	-	Annealed single crystal
Niobium VI	0.935	106	Material Research Corp.	-	Triply zone-refined polycrystal
Nb-Fe	1.09	52	Material Research Corp.	0.01% Fe doping	Polycrystal

Table I (continued)

	Amount (mole)	$R_{300}/R_{4.2}$	Source	Purity	Physical Form
Nb-Zr	1.25	56	Material Research Corp.	0.1% Zr doping	Polycrystal
Tantalum I	0.185	400	Westinghouse Research Laboratories	-	Two zone-refined single crystals
Tantalum II	1.02	90	Material Research Corp.	99.995%	Triply zone-refined single crystal
Tantalum III	1.22	72	Union Carbide	99.9%	Polycrystal

Table II Vanadium sample impurities (ppm) from the supplier.

O_2	100
N	30
H	0.7
C	65
Fe	20
Ni	<10
Mg	< 5
Si	25
Mo	15

Table III Heat capacities of vanadium

	Vanadium I	Vanadium II
$R_{300}/R_{4.2}$	13.3	-
T_c	5.084	5.068
γ(mJ/mole-°K^2)	9.64	9.64
$\frac{C_s - C_n}{\gamma T_c}$	1.50	1.49

Table IV Summary of calorimetric and related data for vanadium

Measurement	$R_{300}/R_{4.2}$	Range (°K)	$H_c(0)$ (gauss)	T_c (°K)	γ(mJ $°K^{-2}$ $mole^{-1}$)	Θ_0(°K)
Elastic constant[a] Alers and Waldorf	150	4.2				400
Calorimetric[b] Keesom and Radebaugh	150	0.7-7	1427	5.37	9.92	399
Calorimetric[c] Corak, Goodman et al.	12.5	1.1-5	1310	5.03	9.26±0.03	338±5
Calorimetric[d] Worley, Zemansky, and Boorse	-	1.7-5	1340	4.89	8.86	273
Critical field[e] Jean Mueller	-	1.3-5	1170	5.30		
This work	13.3	0.3-25	1337	5.068	9.64	400

[a] G. A. Alers and D. L. Waldorf, Phys. Rev. Letters 6, 677 (1961).

[b] R. Radebaugh and P. H. Keesom, Phys. Rev. Letters 13, 685 (1964).

[c] W. S. Corak, B. B. Goodman, C. B. Satterthwaite and A. Wexler, Phys. Rev. 102, 656 (1956).

[d] R. D. Worley, M. W. Zemansky, and H. A. Boorse, Phys. Rev. 99, 447 (1955).

[e] J. Mueller, Helv. Phys. Acta. 32, 141 (1959).

Table V

Niobium sample impurities (ppm). Figures enclosed in brackets give results of neutron activation analysis. Figures not enclosed in brackets give the amount of the impurity reported by the supplier of the sample. No entry indicates that the supplier did not give an analysis.

	Nb I	Nb II	Nb III	Nb IV	Nb V	Nb VI	Nb-Zr	Nb-Fe
Interstitial C, H, O, N	< 10			< 10	High	36		
Ta	<3500 {5380}	1000 {1330}	{73}	<3500	<3500	100		
W	{26.6}	300 {358}	{57}			7		
Si	< 20	300		< 20	< 20	< 0.6		
Ti		100				<0.02		
V		200				< 0.8		
Fe	ND	100		ND	ND	0.12		50-100
Ni		200				<0.15		
Zr		200				< 0.3	1000	
Mo	< 10			< 10	< 10			

Table VI Heat capacities of niobium and niobium alloys.

	Nb I	Nb II	Nb III	Nb IV	Nb V	Nb VI	Nb-Fe	Nb-Zr
$R_{300}/R_{4.2}$	110	25	279	110	61.6	106	52	56
T_c	9.261	9.128	9.278	9.261	9.233	9.261	9.225	9.26
maximum width of transition	0.020	0.086	0.040	0.020	0.065	0.020	0.13	0.15
γ(mJ/mole°K^2)	7.85	7.79	7.85	7.85	-	-	7.79	7.8
$\frac{C_s(T_c)-C_n(T_c)}{\gamma T_c}$	1.80	1.79	1.86	1.80	1.83	-	-	-

Table X. Energy gap for vanadium, niobium and tantalum at 0°K in units of kT_c

Measurement	Vanadium	Niobium	Tantalum
Goodman[a] (Calorimetric)	3.5		3.6
Keesom[b] (Calorimetric)	3.28		
Brewster[c] (Ultrasonic)	3.4		
Richard and Tinkham[d] (IR absorption)		2.8	
Levy[e] (Ultrasonic)	3.5	3.7	3.4-3.5
Bohm[f] (Ultrasonic)	3.1-3.4		
Dietrich[g] (Tunnelling)			3.65
Giaever[h] (Tunnelling)	3.4	3.6	3.5
Townsend and Sutton[i] (Tunnelling)		3.84	
Mendelssohn[j] (Thermal conductivity)		3.8	
Dobbs and Perez[k] (Ultrasonic)		3.77(100) 3.74(111) 3.65(110)	
Neugebauer and Ekvall[l] (Tunnelling)	3.4	3.6	3.5
This work (Calorimetric)			
(1) $\frac{b}{1.44} \times 3.52$	3.5	3.6	3.55
(2) $\frac{4}{\sqrt{3}} \pi \left(\frac{H_o^2 V}{8\pi\gamma T_c^2}\right)^{1/2}$	3.56	3.69	3.55

Table X (continued)

a. W. S. Corak, B. B. Goodman, C. B. Satterthwaite and A. Wexler, Phys. Rev. 102, 656 (1956).

b. J. L. Brewster, (Ph.D. Thesis), Department of Physics, University of California, Los Angeles (1962).

c. M. Levy, (Ph.D. Thesis), Department of Physics, University of California, Los Angeles (1962).

d. D. White, C. Chou and H. S. Johnston, Phys. Rev. 109, 797 (1958).

e. P. H. Keesom and R. Radebaugh, Phys. Rev. Letters 13, 685 (1964).

f. H. V. Bohm and N. H. Horwitz, Eighth International Conference on Low Temperature Physics, (Butterworth's Scientific Publications, Ltd., London, 1962).

g. I. Dietrich, Eighth International Conference on Low Temperature Physics, (Butterworth's Scientific Publications, Ltd., London, 1962).

h. I. Giaever, Eighth International Conference on Low Temperature Physics, (Butterworth's Scientific Publications, Ltd., London, 1962).

i. P. Townsend and S. Sutton, Phys. Rev. 128, 591 (1962).

j. K. Mendelssohn IBM J. of Research and Development 6, 27 (1962).

k. E. R. Dobbs and J. M. Perez, International Conference on the Science of Superconductivity, Colgate University, August 1963.

l. C. A. Neugebauer and R. A. Ekvall, J. Applied Phys. 35, 547 (1964).

REFERENCES

1. G. M. Eliashberg, Zh. Eksperim. i Teor. Fiz. 43, 1005 (1962); (Engl. Trans.: Soviet Phys. -JETP 16, 780 (1963).
2. J. Bardeen, L. N. Cooper, and J. R. Schrieffer, Phys. Rev. 108, 1175 (1957).
3. G. A. Alers and D. L. Waldorf, Phys. Rev. Letters 6, 677 (1961).
4. H. R. O'Neal and N. E. Phillips, Phys. Rev. 137, A748 (1965).
5. R. P. Worley, M. W. Zemansky, H. A. Boorse, Phys. Rev. 99, 447 (1955).
6. W. S. Corak, B. B. Goodman, C. B. Satterthwaite, and A. Wexler, Phys. Rev. 102, 656 (1956).
7. H. Suhl, B. T. Matthias, and L. R. Walker, Phys. Rev. Letters 3, 552 (1959).
8. N. M. Senozan, (PhD. Thesis) University of California, Berkeley (1965).
9. J. C. M. Ho, (PhD. Thesis) University of California, Berkeley (1965).
10. J. P. Franck, F. D. Manchester, and D. L. Martin, Proc. Roc. Soc. A, 263, 494 (1961).
11. J. W. Edwards, R. Speiser, H. L. Johnston, J. Appl. Phys. 22, 424 (1951); and D. I. Bolef, J. Appl. Phys. 32, 100 (1961).
12. B. B. Goodman, Compt. Rend. 246, 3031 (1958).
13. P. H. Keesom and R. Radebaugh, Phys. Rev. Letters 13, 685 (1964).
14. H. A. Leupold and H. A. Boorse, Phys. Rev. 134, A 1322 (1964).
15. T. McConville and B. Serin, International Conference on the Science of Superconductivity, Colgate University, August 1963 (unpublished).
16. T. F. Stromberg and C. A. Swenson, Phys. Rev. Letters 9, 370 (1962).
17. J. C. Swihart, Phys. Rev. 131, 73 (1963).

18. E. A. Lynton, B. Serin, and M. Zucker, J. Phys. Chem. Solids 3, 165 (1957).

19. P. W. Anderson, J. Phys. Chem. Solids 11, 26 (1959).

20. D. Markowitz and L. P. Kadanoff, Phys. Rev. 131, 563 (1963).

21. B. W. Maxfield and W. L. McLean, Phys. Rev. 139, A1515 (1965).

22. J. I. Budnick, Phys. Rev. 119, 1578 (1960).

23. E. Fawcett, Phys. Rev. 128, 154 (1962).

24. N. E. Phillips, M. H. Lambert and W. R. Gardner, Rev. Mod. Phys. 36, 131 (1964).

25. B. J. C. Van der Hoeven and P. H. Keesom, Phys. Rev. 135, A631 (1964).

26. B. J. C. Van der Hoeven and P. H. Keesom, Phys. Rev. 137, A103 (1965).

27. A. T. Hirshfeld, H. A. Leupold and H. A. Boorse, Phys. Rev. 127, 1501 (1962).

28. B. J. C. Van der Hoeven and P. H. Keesom, Phys. Rev. 134, A1320 (1964).

29. For a more complete list of $(C_s-C_n)/\gamma T_c$ of other metals, please refer to R. H. Batt, (PhD. Thesis) University of California, Berkeley (1964).

30. J. Bardeen, private communication.

31. R. D. Worley, M. W. Zemansky and H. A. Boorse, Phys. Rev. 99, 447 (1955).

32. C. A. Bryant and P. H. Keesom, Phys. Rev. 123, 491 (1961).

33. L. Y. L. Shen, N. M. Senozan and N. E. Phillips, Phys. Rev. Letters 14, 1025 (1965).

34. J. W. Garland, Phys. Rev. Letters 11, 111 (1963).

35. C. C. Sung and L. Y. L. Shen, to be published.

36. J. M. Ziman, Electrons and Phonons, (Clarendon Press, Oxford, 1960).

37. R. G. Chambers, Proc. Roy. Soc. A215, 481 (1963).

FIGURE CAPTIONS

Fig. 1 Heat capacity of copper between 0.3 and 4°K.

Fig. 2 Variation of the Debye temperature of copper with temperature.

Fig. 3 The system for measuring residual resistivity. The same superconducting magnet was used in the heat capacity measurements.

Fig. 4 The heat capacity of vanadium. The slopes of the solid lines represent $C_{\ell n}$.

Fig. 5 The heat capacities of two different vanadium samples near the transition temperature.

Fig. 6 The superconducting-state electronic heat capacity of vanadium.

Fig. 7 The lattice heat capacity of normal vanadium.

Fig. 8 The deviations of the critical fields of vanadium, niobium, and tantalum from a parabola.

Fig. 9 The heat capacities of different-purity niobium samples. The slopes of the solid lines represent $C_{\ell n}$.

Fig. 10 The heat capacities of three niobium samples near the transition temperature.

Fig. 11 The superconducting-state electronic heat capacities of different-purity niobium samples. The dashed curve represents the expression $C_{es}/\gamma T_c = 7.0 \exp(-1.46\ T_c T/T) + 0.0038\ (0.25\ T_c/T)^2 \exp(0.25\ T_c/T)\ (1 + \exp(0.25\ T_c/T))^{-2}$.

Fig. 12 The superconducting-state electronic heat capacities of Nb IV, Nb V, Nb VI, Nb-Zr and Nb-Fe.

Fig. 13 The heat capacities of different-purity tantalum samples. The slopes of the solid lines represent $C_{\ell n}$.

Fig. 14 The lattice heat capacity of normal tantalum.

Fig. 15 The heat capacities of three tantalum samples near the transition temperature.

Fig. 16 The superconducting-state electronic heat capacities of different-purity tantalum samples.

Fig. 17 The change of transition temperature vs the reciprocal of the residual resistance for niobium.

Fig. 18 The change of transition temperature vs the reciprocal of the risidual resistance for tantalum. The straight line is taken from Budnick's work.[21]

Fig. 19 Variation of the Debye temperature of vanadium with temperature.

Fig. 20 Variation of the Debye temperature of tantalum with temperature.

Fig. 21 The calculation of the superconducting electronic heat capacity for different $\Delta_s(0)$'s based on Eq. 13. The points are the experimental data of Nb I and Nb II.

Fig. 22 The value of $\Delta_s(T)$. The change of α between 0.3 and 0.7 does not affect the general feature of the fit with experimental data.

II. THE HEAT CAPACITY OF FERROMAGNETIC CHROMIC TRIBROMIDE

A. INTRODUCTION

Ferromagnetic $CrBr_3$ (Curie temperature = 37°K) is one of the few known ferromagnetic insulators. These materials are ideal for testing spin-wave theories of varying degrees of sophistication, because the spins are localized on lattice sites. The magnetic properties of $CrBr_3$ have been well-studied, partly because it was the first such material to be discovered, and partly because its Curie temperature is in a convenient region. The anisotropic magnetization was measured by a static method (Tsubokawa)[1] and by ferromagnetic resonance (Dillon).[2] The temperature dependence of the magnetization was studied via the Cr^{53} nuclear magnetic resonance from 1 to 4°K (Gossard, Jaccarino, and Remeika)[3], and from 1 to 20°K (Davis and Narath).[4] Although $CrBr_3$ has the $R\bar{3}$ structure in which hexagonal layers of Cr ions are separated by two hexagonal closed packed layers of Br ions, the simplified model suggested by Gossard, Jaccarino, and Remeika (GJR)[3] has been applied very successfully to magnetization data. In this model there are two exchange parameters J_t and J_ℓ, that represent exchange coupling in the hexagonal basal plane and between layers, and an anisotropy field H_A.

A test of whether the spin wave theory can provide a satisfactory interpretation of the heat capacity data as well as the magnetization data by using the same parameters is of particular interest. Because $CrBr_3$ has no conduction electrons, and therefore no electronic heat capacity, the analysis of the low-temperature heat capacity is simpler than it would be for a metal. On the other hand, the temperature dependence of the lattice heat capacity can be expected to be relatively complicated due to the complex, layer-like, crystal structure.

If we separate the heat capacity into magnetic and lattice contributions, the magnetic heat capacity should decrease in a magnetic field and the lattice heat capacity remain unchanged. By measuring the heat capacity both in zero and in high magnetic fields, we hoped to test the possibility of separating the heat capacity into a field-independent lattice contriubtion and a field-dependent magnetic contribution calculated from spin-wave theory.

B. EXPERIMENTAL PROCEDURES

The flake-like, polycrystalline $CrBr_3$ sample was kindly provided by Dr. A. C. Gossard and Dr. J. P. Remeika of the Bell Telephone Laboratories. $CrBr_3$ decomposes slowly at room temperature by losing bromine. We preserved the sample in a sealed tube at 78°K to prevent any change in composition with time. Before and after the calorimetric measurements, the bromine content was chemically analyzed with a result corresponding to 99.8% $CrBr_3$.

We tightly packed the small crystals of $CrBr_3$ (0.039 mole) inside a 1/2" O.D., cylindrical, thin-walled, copper container that had been machined from a single piece of 99.9999% copper. The calorimeter was held in place by the same copper rings with heater and thermometer assembly that was described in Part I. The thermal contact between flakes was provided by wetting the crystals with chemically-inert Dow Corning 703 silicone diffusion pump oil. The heat capacity of the silicone oil is listed in the Appendix. The addenda correction includes 16 g. of copper from the container, 0.73 g. of silicone oil, and the addenda from thermometer etc. obtained from Part I. The total addenda was 14% of the measured value at 0.4°K where the zero-field heat capacity of $CrBr_3$ attained its smallest value. In the high magnetic

field, there is a nuclear heat capacity of the copper container. This was estimated to be $0.08/T^2$ mJ/deg for each mole of $CrBr_3$ in 27 kG. This additional correction of addenda was made for measurements in the magnetic fields.

The heat capacity was measured by the same method described in Part I. We applied a series of uniform magnetic field from 20.4 to 27 kG on $CrBr_3$ after the zero-field measurements. Thermal relaxation was rapid except for the zero-field measurement below 0.5°K. At the lowest temperature a thermal relaxation time of approximately one minute was observed. It seems probable that this is the spin-lattice relaxation time of the Br nuclei.[5]

C. RESULT AND COMPARISON WITH SPIN WAVE THEORY

We report here the heat capacity of $CrBr_3$ from 0.3 to 25°K in 0, 20.4, and 27 kG fields. The zero field heat capacity agreed with the measurements by Jennings and Hansen[6] above 14°K where the two measurements overlapped.

The heat capacity of $CrBr_3$ below 5°K in the zero field is plotted as $C/T^{3/2}$ vs $T^{3/2}$ in Fig. 1. Figure 2 extends the heat capacity to 10°K in zero and 27 kG on the same type of plot. We assume that the total heat capacity is a sum of lattice and magnetic contributions

$$C = C_\ell + C_{mag}.$$

At low enough temperatures, C_ℓ is proportional to T^3 and C_{mag} is proportional to $T^{3/2}$ for an ideal ferromagnet. This type of temperature dependence gives a straight line on the $C/T^{3/2}$ vs $T^{3/2}$ plot, where the slope and the intercept determine C_ℓ and C_{mag}, respectively.

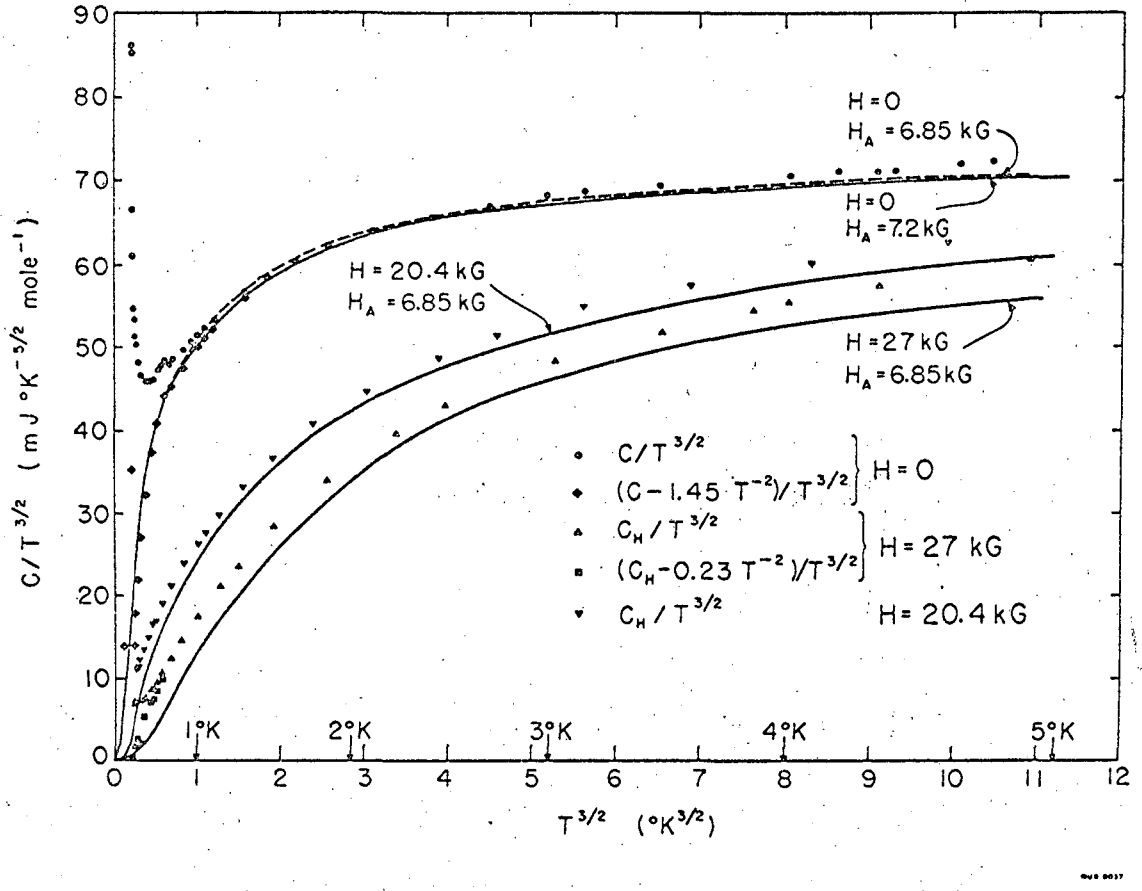

Fig. 1

The heat capacity of $CrBr_3$ from 0.3°K to 5°K in 0, 20.4 and 27 kG. The dashed curve represents the calculation from Eq.(2). The solid curve that passes through the zero-field data is obtained from Eq.(2) using a different H_A. The solid curves near the high-field data are calculated from Eq.(3).

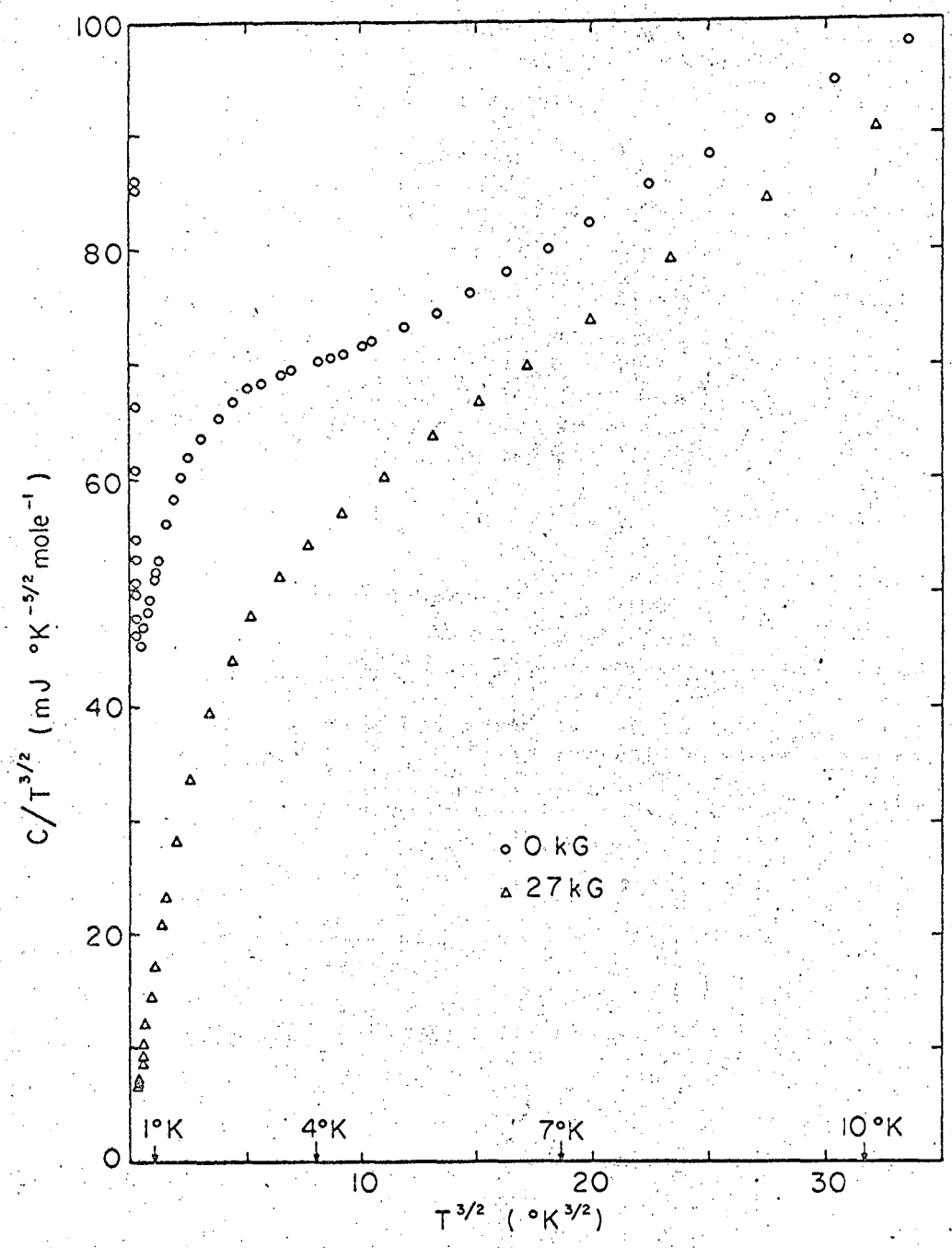

Fig. 2

The heat capacity of $CrBr_3$ from 0.3 to 10°K.

In the present case, there are three reasons to expect a deviation from the linear behavior. First at the lowest temperature, we have the nuclear heat capacity from the hyperfine field acting on the magnetic moment of the nuclei. The nuclear heat capacity has a T^{-2} dependence. Second, in the presence of an anisotropy field H_A, the magnetic heat capacity is proportional to $T^{3/2}$ multiplied by a function of H_A/T that decreases exponentially to zero as T tends to zero. Third, the lattice heat capacity is proportional to T^3 only in the limit T goes to zero, and for a complex crystal structure such as that of $CrBr_3$ it is not possible to predict the temperature range in which this is a good approximation.

The nuclear heat capacity in zero field was determined to be $1.45/T^2$ mJ/mole-deg by subtracting out the calculated C_{mag} below 1°K. The nuclear heat capacity first decreased in a magnetic field reaching a minimum at 23 kG and increased to $0.23/T^2$ mJ/mole-deg in 27 kG. This could be explained by a negative hyperfine field of 23 kG. But the zero-field nuclear heat capacity was 5 times larger than the heat capacity calculated from the known nuclear energy levels of Br^{79}, Br^{81}, and Cr^{53}. We were not able to explain the origin of the T^{-2} term in zero magnetic field or its field dependence. It seems clear that this term should be subtracted from the total before attempting an analysis of C_ℓ and C_{mag}. The total heat capacity less the contribution that is proportional to T^{-2} is presented in Figs. 1 and 4 for zero and 27 kG field.

In the low temperature limit, C_{mag} depends on H_A and the product $J_\ell^{1/2} J_t$. H_A was reported by Dillon from ferromagnetic resonance,[2] whereas J_ℓ and J_t were determined by Davis and Narath from the temperature dependence

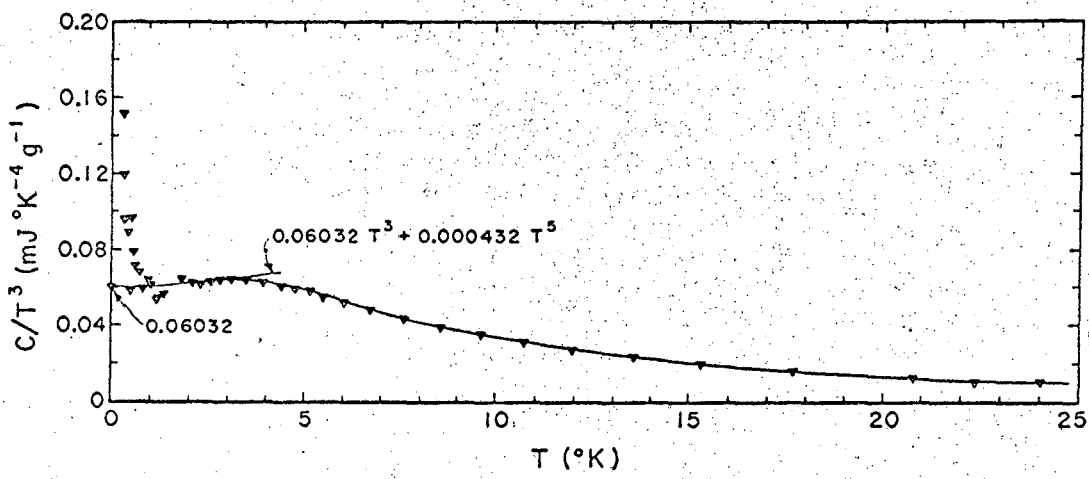

Fig. 4

The heat capacity of Dow Corning 703 silicone diffusion pump oil.

of Cr^{53} zero-field nuclear magnetic resonance frequency.[4]

The curves in Fig. 1 were calculated by Dr. D. L. Mills[7] from the simplified spin wave model of Gossard, Jaccarino, and Remeika.[3] By using their notation, the dispersion relation to order k^2 where $\underline{k}$ is the wave vector with components k_x, k_y, k_z is given by

$$\omega(\underline{k}) = Hg\beta + SJ_\ell c^2 k_z^2 + \frac{3}{4} SJ_t a^2 (k_x^2 + k_y^2).$$

In the above equation, $S = 3/2$ is the spin of Cr^{+3} ion, g is very close to 2 for the ground state[4] A_2 of Cr ion, β is the Bohr magneton, a and c are the lattice parameters, and H is the magnetic field acting on the spin.

The internal energy per unit volume u of the spin waves which obey Bose statistics becomes

$$u = \frac{1}{V} \sum_{k} \frac{\omega(\underline{k})}{\exp\,(\omega(\underline{k})/kT)-1}$$

where V is the volume of the unit cell. Replacing the summation by integration of $\underline{k}$ from zero to infinity we obtain the total internal energy U as

$$U = \frac{15\sqrt{3}\,R}{64\pi^{3/2} S^{3/2} J_\ell^{1/2} J_t} \left[\frac{Hg\beta}{k} T^{3/2} \sum_{m=1}^{\infty} \frac{e^{-mHg\beta/kT}}{m^{3/2}} + \frac{3}{2} T^{5/2} \sum_{m=1}^{\infty} \frac{e^{-mHg\beta/kT}}{m^{5/2}} \right]$$

where R is the gas constant. Differentiating U with respect to T, we get the heat capacity in magnetic field H

$$C_{mag} = \frac{15\sqrt{3}\,\zeta(5/2)R}{64\pi^{3/2}S^{3/2}J_\ell^{1/2}J_t}\,T^{3/2}\,F\left(\frac{H}{T}\right) \qquad (1)$$

where

$$F(H/T) = \frac{1}{\zeta(5/2)}\left[\frac{4}{5}\left(\frac{Hg\beta}{kT}\right)^2 \sum_{m=1}^{\infty} \frac{e^{-mHg\beta/kT}}{m^{1/2}}\right.$$

$$\left. + \frac{4}{5}\left(\frac{Hg\beta}{kT}\right) \sum_{m=1}^{\infty} \frac{e^{-mHg\beta/kT}}{m^{3/2}} + \sum_{m=1}^{\infty} \frac{e^{-mHg\beta/kT}}{m^{5/2}}\right]$$

with Riemann zeta function $\zeta(5/2) = 1.341$. When we take $J_\ell = 0.497°K$ and $J_t = 0.825°K$ from the work of Davis and Narath,[4] and anistropy field $H = H_A = 6.85$ kG from the work of Dillon,[2] the magnetic heat capacity of $CrBr_3$ in zero external magnetic field becomes

$$C_{mag} = 76.07\,T^{3/2}\,F\left(\frac{6.85}{T}\right) mJ/mole\text{-}deg. \qquad (2)$$

This is shown as the dashed curve in Fig. 1. The function $F(H/T)$, as a function of H/T is taken from the calculation of Mills and shown on Fig. 3.

Although the original purpose of the measurements in an external field was to find C_ℓ by freezing out the spin-wave heat capacity, the difficulties in calculating C_{mag} for the experimental conditions prevent an accurate analysis of these measurements. For the available magnetic field and temperature range, where H/T was less than 50 kG/°K, $F(H/T)$ was always larger than 0.01, and C_{mag} was not negligible compared with possible values of C_ℓ at all temperatures. Furthermore, the complicated way in which H_e and the anisotropy energy (represented by H_A) combines

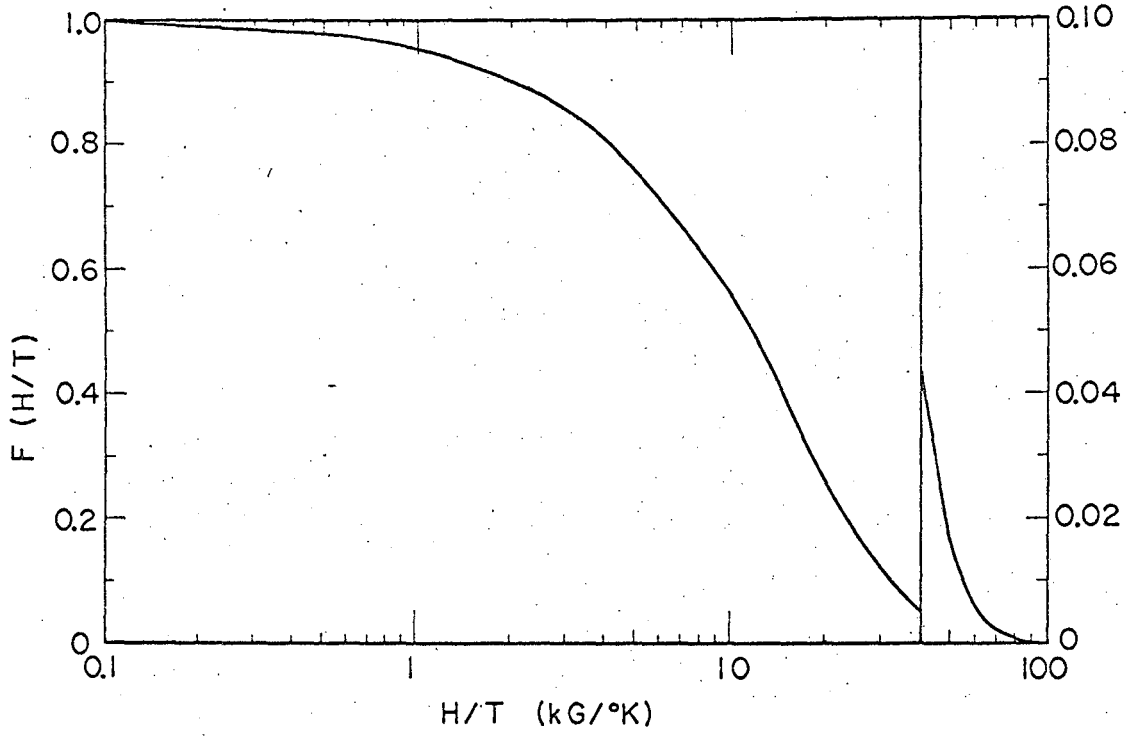

Fig. 3

The function F(H/T) from the work of D. L. Mills.

to produce an effective field, H_{eff} for a crystal with an arbitrary orientation relative to H_e, makes the calculation of $F(H_{eff}/T)$ extremely difficult. If H_A is not negligible compared with H_e, the spin wave dispersion relation becomes a function of H_e, H_A, the wave vector $\underline{k}$, and the angle between H_e and the c-axis (the easy direction of magnetization). The correct C_{mag} involves first a proper averaging of $\underline{k}$ using the dispersion relation for each direction of the crystalline orientation and then averaging over the various crystalline directions. In view of other difficulties in the interpretation of the data, this complex calculation was not considered worthwhile. First, the packed $CrBr_3$ flakes might not have random orientations. Second, the demagnetization field cannot be included exactly because of the cylindrical geometry and the polycrystalline nature of the sample, but it can create corrections to the applied field and the field acting on the spins of the order of 1 kG.

The empirical formula

$$C_H = 76.07\, T^{3/2} \cdot \frac{1}{2} \cdot \left(F\left(\frac{H - H_A}{T}\right) + F\left(\frac{H + H_A}{T}\right)\right) \text{ mJ/°K-mole} \qquad (3)$$

which was obtained by taking $H_{eff} = H_e + H_A$ for half of the sample and $H_{eff} = H_e - H_A$ for the other half fit the 20.4 and 27 kG data fairly well as shown in Fig. 1. If the c-axis is parallel to H_e, H_{eff} is indeed $H_e + H_A$, but for the c-axis perpendicular to H_e, H_{eff} becomes $(H_e(H_e - H_A))^{1/2}$.[8]

Since we cannot calculate C_{mag} in the magnetic fields satisfactorily, C_ℓ is rather uncertain and further analysis must be restricted to the zero-field data. Below 4°K, the validity of Eq. (2) where we neglected the k^4 term in the dispersion formula and Brillouin zone-bouhdary effects is supported by GJR's analysis of magnetization data.[3] The neglect of the

of Cr^{53} zero-field nuclear magnetic resonance frequency.[4]

The curves in Fig. 1 were calculated by Dr. D. L. Mills[7] from the simplified spin wave model of Gossard, Jaccarino, and Remeika.[3] By using their notation, the dispersion relation to order k^2, where $\underline{k}$ is the wave vector with components k_x, k_y, k_z is given by

$$\omega(\underline{k}) = Hg\beta + SJ_\ell c^2 k_z^2 + \frac{3}{4} SJ_t a^2 (k_x^2 + k_y^2).$$

In the above equation, $S = 3/2$ is the spin of Cr^{+3} ion, g is very close to 2 for the ground state[4] A_2 of Cr ion, β is the Bohr magneton, a and c are the lattice parameters, and H is the magnetic field acting on the spin.

The internal energy per unit volume u of the spin waves which obey Bose statistics becomes

$$u = \frac{1}{V} \sum_{\underline{k}} \frac{\omega(\underline{k})}{\exp\,(\omega(\underline{k})/kT)-1}$$

where V is the volume of the unit cell. Replacing the summation by integration of $\underline{k}$ from zero to infinity we obtain the total internal energy U as

$$U = \frac{15\sqrt{3}\,R}{64\pi^{3/2} S^{3/2} J_\ell^{1/2} J_t} \left[\frac{Hg\beta}{k} T^{3/2} \sum_{m=1}^{\infty} \frac{e^{-mHg\beta/kT}}{m^{3/2}} + \frac{3}{2} T^{5/2} \sum_{m=1}^{\infty} \frac{e^{-mHg\beta/kT}}{m^{5/2}} \right]$$

where R is the gas constant. Differentiating U with respect to T, we get the heat capacity in magnetic field H

$$C_{mag} = \frac{15\sqrt{3}\,\zeta(5/2)R}{64\pi^{3/2}S^{3/2}J_\ell^{1/2}J_t}\,T^{3/2}\,F\left(\frac{H}{T}\right) \qquad (1)$$

where

$$F(H/T) = \frac{1}{\zeta(5/2)}\left[\frac{4}{5}\left(\frac{Hg\beta}{kT}\right)^2 \sum_{m=1}^{\infty} \frac{e^{-mHg\beta/kT}}{m^{1/2}}\right.$$

$$\left. + \frac{4}{5}\left(\frac{Hg\beta}{kT}\right) \sum_{m=1}^{\infty} \frac{e^{-mHg\beta/kT}}{m^{3/2}} + \sum_{m=1}^{\infty} \frac{e^{-mHg\beta/kT}}{m^{5/2}}\right]$$

with Riemann zeta function $\zeta(5/2) = 1.341$. When we take $J_\ell = 0.497°K$ and $J_t = 0.825°K$ from the work of Davis and Narath,[4] and anistropy field $H = H_A = 6.85$ kG from the work of Dillon,[2] the magnetic heat capacity of $CrBr_3$ in zero external magnetic field becomes

$$C_{mag} = 76.07\,T^{3/2}\,F\left(\frac{6.85}{T}\right) \text{mJ/mole-deg}. \qquad (2)$$

This is shown as the dashed curve in Fig. 1. The function $F(H/T)$, as a function of H/T is taken from the calculation of Mills and shown on Fig. 3.

Although the original purpose of the measurements in an external field was to find C_ℓ by freezing out the spin-wave heat capacity, the difficulties in calculating C_{mag} for the experimental conditions prevent an accurate analysis of these measurements. For the available magnetic field and temperature range, where H/T was less than 50 kG/°K, $F(H/T)$ was always larger than 0.01, and C_{mag} was not negligible compared with possible values of C_ℓ at all temperatures. Furthermore, the complicated way in which H_e and the anisotropy energy (represented by H_A) combines

second order term in their formula constitutes less than 5% error at 2°K and 10% at 4°K. Between 1 and 2°K the theory gives a reliable C_{mag}. In this temperature region, we believe C_ℓ is negligible compared with C_{mag} because, for $kT \gtrsim g\beta H_A$, the ratio of C_ℓ to C_{mag} is of the order of $\left(\frac{T}{\Theta_o}\right)^3 / \left(\frac{T}{T_c}\right)^{3/2} \sim 0.0001\ T^{3/2}$ where Θ_o and T_c are the Debye and Curie temperatures. Jennings and Hansen[6] proposed an empirical formula for C_ℓ, based on their heat capacity measurements above 14°K, which gives a heat capacity in this region corresponding to $\Theta_o = 118$°K and 2% of the measured heat capacity at 1°K. Since their formula was obtained by fitting Debye functions to the heat capacity at temperatures for which $CrBr_3$ may have a large T^5 term in C_ℓ, it probably overestimates the low-temperature T^3 term. The experimental data is below C_{mag} calculated from Eq. (2), showing that Eq. (2) must give an overestimate. Since we have already chosen J_ℓ and J_t given by Davis and Narath,[4] and since only a narrow temperature region is involved, we have varied only H_A in trying to fit the data. As shown by the solid curve in Fig. 1, $H_A = 7.2$ kG does give a good fit to the zero-field data.

Ferromagnetic resonance determined H_A to be 6.85 kG[2] which differed by a factor of 2 from the results of static magnetization measurement.[1] Whether the macroscopically determined H_A is the same as the H_A in spin wave, theory was solely determined by the temperature dependence of NMR frequency $\nu(T)$, where $H_A = 6.85$ kG was used as a fixed parameter. However, the magnetic heat capacity is more sensitive to H_A than $\nu(T)$, because as T tends to 0°K the leading term of the latter is

$$[\nu(0) - \nu(T)]/\nu(0) \doteq 0.000976\ T^{3/2}\ e^{-H_A g\beta/kT}$$

which is less dependent on H_A than

$$C_{mag}(T) = 46.5\ T^{-1/2} \left(\frac{H_A g\beta}{k}\right)^2 e^{-H_A g\beta/kT} \quad mJ/mole\text{-}deg$$

Furthermore, our measurements extend to relatively low temperatures where the effect of H_A is large. We conclude that there is a small discrepancy in H_A between the measured magnetic heat capacity and ferromagnetic resonance.

In general, it would be of interest to look for a set of values of J_t, J_ℓ, and H_A consistent with both C_{mag} and $\nu(T)$, based on the spin-wave renormalization technique of Davis and Narath.[4] However, in the present case, the uncertainty in C_ℓ would make the result less valuable.

ACKNOWLEDGEMENTS

The author wishes to express his sincere thanks to Professor Norman E. Phillips for his guidance, unfailing interest, and friendship.

The author wishes to thank Dr. G. King and Dr. H. G. Sell of the Westinghouse Electric Corporation for the tantalum I sample used in this experiment; Dr. A. C. Gossard and Dr. J. P. Remeika of Bell Telephone Laboratories for the $CrBr_3$ sample; Dr. J. M. Rowell of Bell Telephone Laboratories for the Pb_{45} - Bi_{55} alloy; Denes Turcsanyi for the annealing of niobium samples.

Theoretical consultations from Dr. C. C. Sung on the calculation of the second energy gap, and from Dr. D. L. Mills on the calculation of the magnetic heat capacity of $CrBr_3$ are greatly appreciated.

Thanks are given to Professor Marvin L. Cohen and Professor C. Kittel for many helpful discussions.

This work was performed under the auspices of the United States Atomic Energy Commission.

APPENDIX

The heat capacity of Dow Corning 703 silicone diffusion pump oil (supplied by Dow Corning Corp., Midland, Michigan) was measured from 0.3 to 25°K. A 60-cm^2, 1-mil thick, copper foil spiral was put inside the calorimeter to aid thermal equilibrium, but long thermal equilibrium time was still observed. The 3.25-g. sample had a thermal relaxation time that varied from 5 minutes at and above 4°K to less than one minute at 0.3°K. The silicone oil contained a small amount of dissolved air while it was exposed to the atmosphere at room temperature.

The result of the heat capacity measurements are shown in Fig. 4. The scatter in the points below 1°K is a consequence of the relatively large electronic heat capacity of the copper container. Below 3°K the date are represented by $0.603T^3 + 0.00043\ T^5$ mJ/deg-g. Above 3°K, the smoothed curve in Fig. 4 was used to represent the heat capacity for the addenda corrections in the $CrBr_3$ run. The valued of C/T^3 are taken from the curve at 1°K interval and listed in Table III.

Table I

Heat Capacity of $CrBr_3$ in Zero Magnetic Field

T (°K)	C (mJ/mole-deg)	T (°K)	C (mJ/mole-deg)
0.3541	18.14	2.7181	299.95
0.3542	17.96	2.9937	352.53
0.3647	14.63	3.163	385.6
0.3700	13.70	3.486	451.0
0.3803	12.85	3.648	485.8
0.3896	12.91	4.017	567.1
0.4008	12.98	4.205	611.2
0.4118	13.24	4.359	645.9
0.4374	13.88	4.418	660.7
0.4763	15.26	4.670	726.0
0.5272	17.49	4.789	756.7
0.5707	19.76	5.205	872.2
0.5996	21.33	5.615	994.0
0.6535	24.92	6.008	1277.4
0.6895	27.66	6.911	1458.8
0.7217	29.63	7.950	1923.6
0.7978	34.51	9.138	2521.4
0.8901	41.61	10.396	3283.8
0.9573	47.28	12.158	4448.6
1.0018	51.47	14.721	6489.1
1.0617	56.92	16.491	8115.6
1.1285	63.62	18.360	9952.7
1.3514	88.49	20.650	12608.
1.5053	107.55	23.077	15829.
1.6786	131.02		
1.8765	159.48		
2.1222	196.91		
2.4365	248.80		

Table II

Heat Capacity of $CrBr_3$ in 27 Kilogauss Field

T (°K)	C (mJ/mole-deg)	T (°K)	C (mJ/mole-deg)
0.380	1.579	3.026	253.0
0.400	1.820	3.494	336.9
0.429	1.957	3.872	413.8
0.468	2.247	4.012	443.8
0.518	2.771	4.361	520.4
0.585	3.785	4.921	658.2
0.603	4.069	5.545	834.4
0.646	4.893	6.107	1009.7
0.697	6.073	6.657	1201.0
0.781	8.437	7.343	1474.4
0.866	12.02	8.167	1850.0
1.015	17.59	9.093	2317.4
1.183	26.85	10.118	2911.1
1.318	35.39	11.348	3676.5
1.552	54.63	12.849	4700.2
1.865	86.00	14.422	5945.0
2.253	133.8	16.679	7930.6
2.508	169.6	19.165	10387.
2.668	193.0	21.858	13353.

Table III

Heat Capacity of Dow Corning 703 Silicone Diffusion Pump Oil

T (°K)	C/T^3 (mJ/ g.-deg)^4
1	0.0607
2	0.0620
3	0.0639
4	0.0629
5	0.0590
6	0.0534
7	0.0471
8	0.0416
9	0.0376
10	0.0341
11	0.0309
12	0.0278
13	0.0249
14	0.0224
15	0.0202
16	0.0182
17	0.0167
18	0.0153
19	0.0141
20	0.0130
21	0.0120
22	0.0112
23	0.0107
24	0.0102

REFERENCES

1. I. Tsubokawa, J. Phys. Soc. Japan 15, 1664 (1960).

2. J. F. Dillon, J. Appl. Phys. Suppl. 33, 1191S (1962).

3. A. C. Gossard, V. Jaccarino, and J. P. Remeika, Phys. Rev. Letters 7, 122 (1961).

4. H. L. Davis, and A. Narath, Phys. Rev. 134, A433 (1964).

5. A. C. Gossard, V. Jaccarino, E. D. Jones, and J. P. Remeika, and R. Slusher, Phys. Rev. 135, A1051 (1964).

6. L. D. Jennings and W. N. Hansen, Phys. Rev. 139, A1694 (1965).

7. D. L. Mills, (Physics Department, University of California, Berkeley), private communication.

8. C. Kittel, Introduction to Solid State Physics, (Wiley) (1956).

FIGURE CAPTIONS

Fig. 1 The heat capacity of $CrBr_3$ from 0.3°K to 5°K in 0, 20.4 and 27 kG. The dashed curve represents the calculation from Eq. (2). The solid curve that passes through the zero-field data is obtained from Eq. (2) using a different H_A. The solid curves near the high-field data are calculated from Eq. (3).

Fig. 2 The heat capacity of $CrBr_3$ from 0.3 to 10°K.

Fig. 3 The function F(H/T) from the work of D. L. Mills.

Fig. 4 The heat capacity of Dow Corning 703 silicone diffusion pump oil.